EGU24-2867
EGU General Assembly 2024

Exploring Extreme Weather and Climate Events with Aeolus 2.0: A Multi-layer moist-convective Thermal Rotating Shallow Water (mcTRSW) Dynamical Core

Masoud Rostami[1,2] and Stefan Petri[1]

[1]Potsdam Institute for Climate Impact Research (PIK), RD1, Germany (rostamimasoud@yahoo.com)

[2]Laboratoire de Météorologie Dynamique (LMD), Sorbonne University (SU), Ecole Normale Supérieure (ENS), Paris, France

Aeolus 2.0 is an open-source numerical atmosphere model with intermediate complexity designed to capture the dynamics of the atmosphere, especially extreme weather and climate events. The model's dynamical core is built on a novel multi-layer pseudo-spectral moist-convective Thermal Rotating Shallow Water (mcTRSW) model, and it utilizes the Dedalus algorithm, renowned for its efficient handling of spin-weighted spherical harmonics in solving pseudo-spectral problems. Aeolus 2.0 comprehensively characterizes the temporal and spatial evolution of key atmospheric variables, including vertically integrated potential temperature, thickness, water vapor, precipitation, and the influence of bottom topography, radiative transfer, and insolation. It provides a versatile platform with resolutions ranging from smooth to coarse, enabling the exploration of a wide spectrum of dynamic phenomena with varying levels of detail and precision.

The model has been utilized to investigate the adjustment of large-scale localized buoyancy anomalies in mid-latitude and equatorial regions, along with the nonlinear evolution of key variables in both adiabatic and moist-convective environments. Our findings highlight the triggering mechanisms of phenomena such as the Madden-Julian Oscillation (MJO) and the circulation patterns induced by temperature anomalies and buoyancy fields. Furthermore, our simulations of large-scale localized temperature anomalies reveal insights into the impact of perturbation strength, size, and vertical structure on the evolution of eddy heat fluxes, including poleward heat flux, energy, and meridional elongation of the buoyancy field. We observe the initiation of atmospheric instability, leading to precipitation systems, such as rain bands, and asymmetric latent heat release due to moist convection in diabatic environments. This study identifies distinct patterns, including the formation of a comma cloud pattern in the upper troposphere and a comma-shaped buoyancy anomaly in the lower layer, accompanied by the emission of inertia gravity waves. Additionally, the role of buoyancy anomalies in generating heatwaves and precipitation patterns is emphasized, particularly in mid-latitude regions.

In summary, Aeolus 2.0, with its specific capabilities, contributes to our understanding of the complex interactions of moist convection, buoyancy anomalies, and atmospheric dynamics, shedding light on the dynamics of extreme weather events and their implications for climate studies.

Exploring Extreme Weather and Climate Events with Aeolus 2.0: A Multi-layer moist-convective Thermal Rotating Shallow Water (mcTRSW) Dynamical Core

Masoud Rostami [1,2] and Stefan Petri [1]

[1] Potsdam Institute for Climate Impact Research (PIK), RD1, Germany
[2] Laboratoire de Météorologie Dynamique (LMD), Sorbonne University (SU), Ecole Normale Supérieure (ENS), Paris, France

Abstract

Aeolus 2.0 is an open-source numerical atmosphere model with intermediate complexity designed to capture the dynamics of the atmosphere, especially extreme weather and climate events. The model's dynamical core is built on a novel multi-layer pseudo-spectral moist-convective Thermal Rotating Shallow Water (mcTRSW) model, and it utilizes the Dedalus algorithm, renowned for its efficient handling of spin-weighted spherical harmonics in solving pseudo-spectral problems. Aeolus 2.0 comprehensively characterizes the temporal and spatial evolution of key atmospheric variables, including vertically integrated potential temperature, thickness, water vapor, precipitation, and the influence of bottom topography, radiative transfer, and insolation. It provides a versatile platform with resolutions ranging from smooth to coarse, enabling the exploration of a wide spectrum of dynamic phenomena with varying levels of detail and precision.

The model has been utilized to investigate the adjustment of large-scale localized buoyancy anomalies in mid-latitude and equatorial regions, along with the nonlinear evolution of key variables in both adiabatic and moist-convective environments. Our findings highlight the triggering mechanisms of phenomena such as the Madden-Julian Oscillation (MJO) and the circulation patterns induced by temperature anomalies and buoyancy fields. Furthermore, our simulations of large-scale localized temperature anomalies reveal insights into the impact of perturbation strength, size, and vertical structure on the evolution of eddy heat fluxes, including poleward heat flux, energy, and meridional elongation of the buoyancy field. We observe the initiation of atmospheric instability, leading to precipitation systems, such as rain bands, and asymmetric latent heat release due to moist convection in diabatic environments. This study identifies distinct patterns, including the formation of a comma cloud pattern in the upper troposphere and a comma-shaped buoyancy anomaly in the lower layer, accompanied by the emission of inertia gravity waves. Additionally, the role of buoyancy anomalies in generating heatwaves and precipitation patterns is emphasized, particularly in mid-latitude regions. In summary, Aeolus 2.0, with its specific capabilities, contributes to our understanding of the complex interactions of moist convection, buoyancy anomalies, and atmospheric dynamics, shedding light on the dynamics of extreme weather events and their implications for climate studies.

POTSDAM INSTITUTE FOR CLIMATE IMPACT RESEARCH

A plethora of related GFD approximations

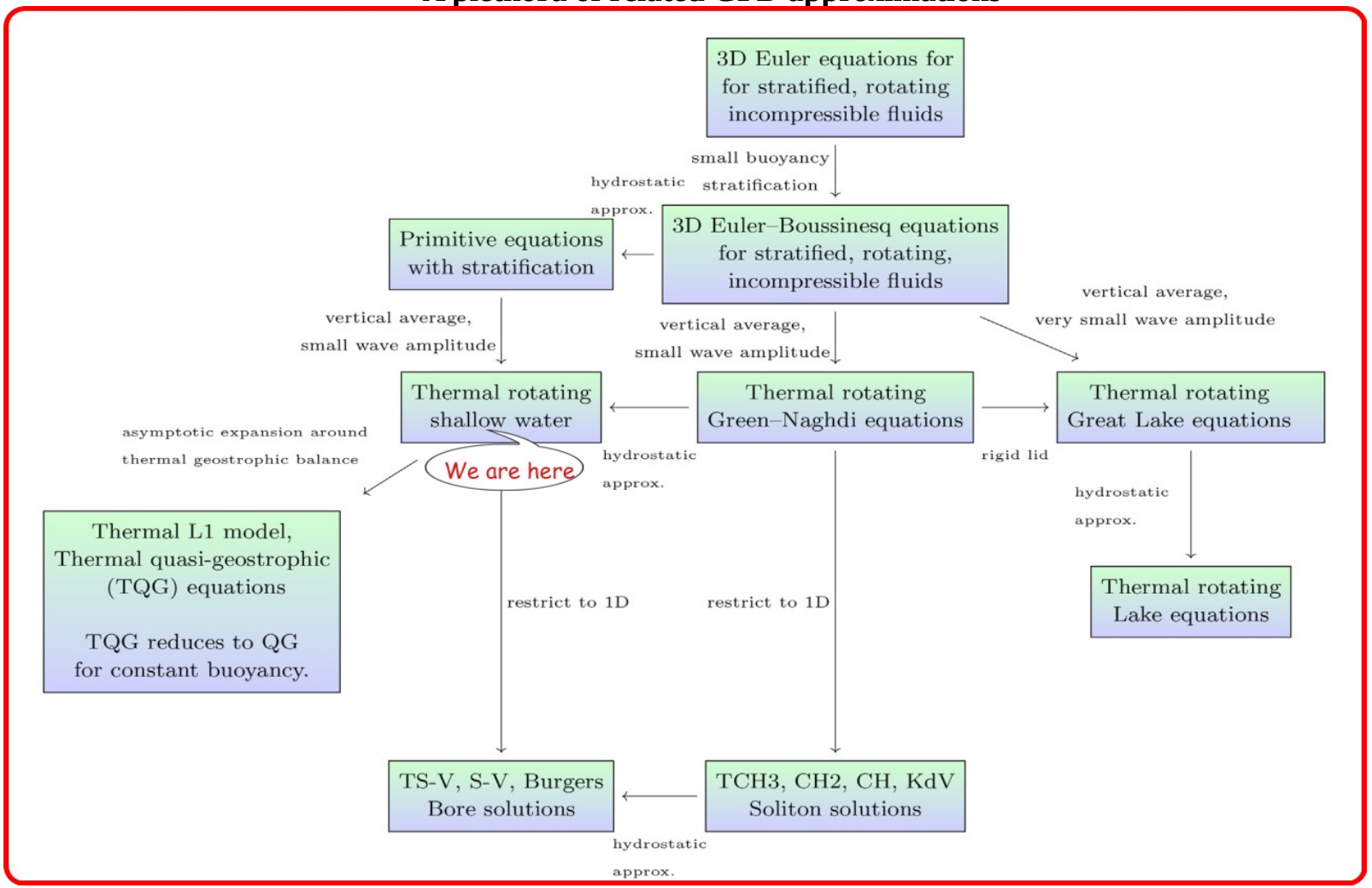

A plethora of related geophysical fluid dynamics (GFD) approximations. This tree diagram describes how the various asymptotic expansions, hydrostatic assumptions and vertical averages lead to a plethora of intimately related GFD approximations. The present work concentrates on the paths leading to the (multi-layer) thermal rotating shallow water (TRSW) model. Figure from Holm et al., (2021).

Layer versus Level Models

Another feature of Aeolus 2.0 is that it is a layer model. Layer models and level models are two approaches used in geophysical fluid dynamics to represent the vertical structure of the atmosphere and oceans. While level models incorporate thermodynamics easily, they are less accurate than layer models, especially at high vertical modes. The difference lies in how these models represent the density profile. In a level model, density is assumed to be continuously stratified, and finite differencing is used at fixed depths. In contrast, a layer model approximates the continuous density profile with a piece-wise constant profile, where the depth of the interfaces can vary with position and time. Accuracy issues in level models arise from the inherent limitations of finite differencing at small scales. In contrast, layer models do not suffer from this problem because the piece-wise constant density profile is physically valid, and the equations of motion precisely represent this particular stratification. The Laplace tidal equations serve as a prominent example that highlights the disparity between layer and level models. These equations, which describe the behavior of tides in the ocean and atmosphere, are a one-layer model with no counterpart in the level model family.

Spin-Weighted Spherical Harmonics

In the numerical methodology employed in Aeolus 2.0, the Dedalus algorithm is utilized. The Dedalus algorithm incorporates the use of spin-weighted spherical harmonics, as documented in the works of Vasil et al. (2019) and Lecoanet et al. (2019). Spin-weighted spherical harmonics were originally introduced by Gelfand and Shapiro (1956) in their studies related to the Lorenz group. One key advantage of utilizing spin-weighted spherical harmonics in combination with spinor basis vectors is the ability to perform differentiation operations on the spherical domain in a manner akin to Fourier series operations. This property enables regular and well-behaved diagonal wavenumber multiplication across the entire sphere, eliminating the necessity for traditional singular gradients at the poles. This advantageous feature enhances the numerical stability and accuracy of calculations performed within the mcTRSW dynamical core on a spherical domain.

How Does Aeolus 2.0 Differ from Others in the Community?

The widely employed Rotating Shallow Water (RSW) model has proven valuable for investigating atmospheric and oceanic flows. It integrates the atmospheric primitive equations using pseudo-height isobaric vertical coordinates, enabling the capture of critical features of large-scale fluid dynamics, including jet streams and Rossby waves. However, the classical RSW model has limitations, notably in its neglect of horizontal gradients of potential temperature and the influence of moist convection, both of which are significant in specific atmospheric and oceanic contexts. These effects, driven by the interaction between temperature and water vapor content, lead to the formation of clouds, precipitation, and other atmospheric features. To overcome these limitations, the mcTRSW dynamical core incorporates horizontal gradients of potential temperature and moist convection, enhancing the accuracy of atmospheric current simulations beyond that of classical RSW models. This, in turn, makes the mcTRSW dynamical core an ideal choice for the investigation of fully nonlinear evolution of large-scale temperature anomalies in a moist-convective or adiabatic environments.

Aeolus 2.0 is indeed a proper choice for studying extreme events such as the Madden-Julian Oscillation (MJO), tropical cyclones, extreme heatwaves, monsoons, and more (Rostami et al., 2023). It offers valuable insights into the intricate interplay between temperature, water vapor content, and large-scale atmospheric dynamics. The model is supported by a theoretical foundation and a historical record of incorporating moist convection in the RSW model (mcRSW), which already accounts for phase transitions of water vapor and the related latent heat release (Bouchut et al., 2009; Rostami & Zeitlin, 2018).

In order to answer scientific questions and trace causalities, the user can configure the various levels of complexity in the model, ranging from a conceptual level to an intermediate level of complexity.

Aeolus 2. 0 Installation and Execution Guide

Aeolus 2.0 has been uploaded to Zenodo and is available via the following link: DOI: 10.5281/zenodo.10054154 (https://zenodo.org/records/10823194). The README file guides users through the installation and execution of Aeolus 2.0. The model utilizes parallel computing, enabling the distribution of computational tasks for faster and more efficient simulations.

The non-adiabatic mechanism of the model

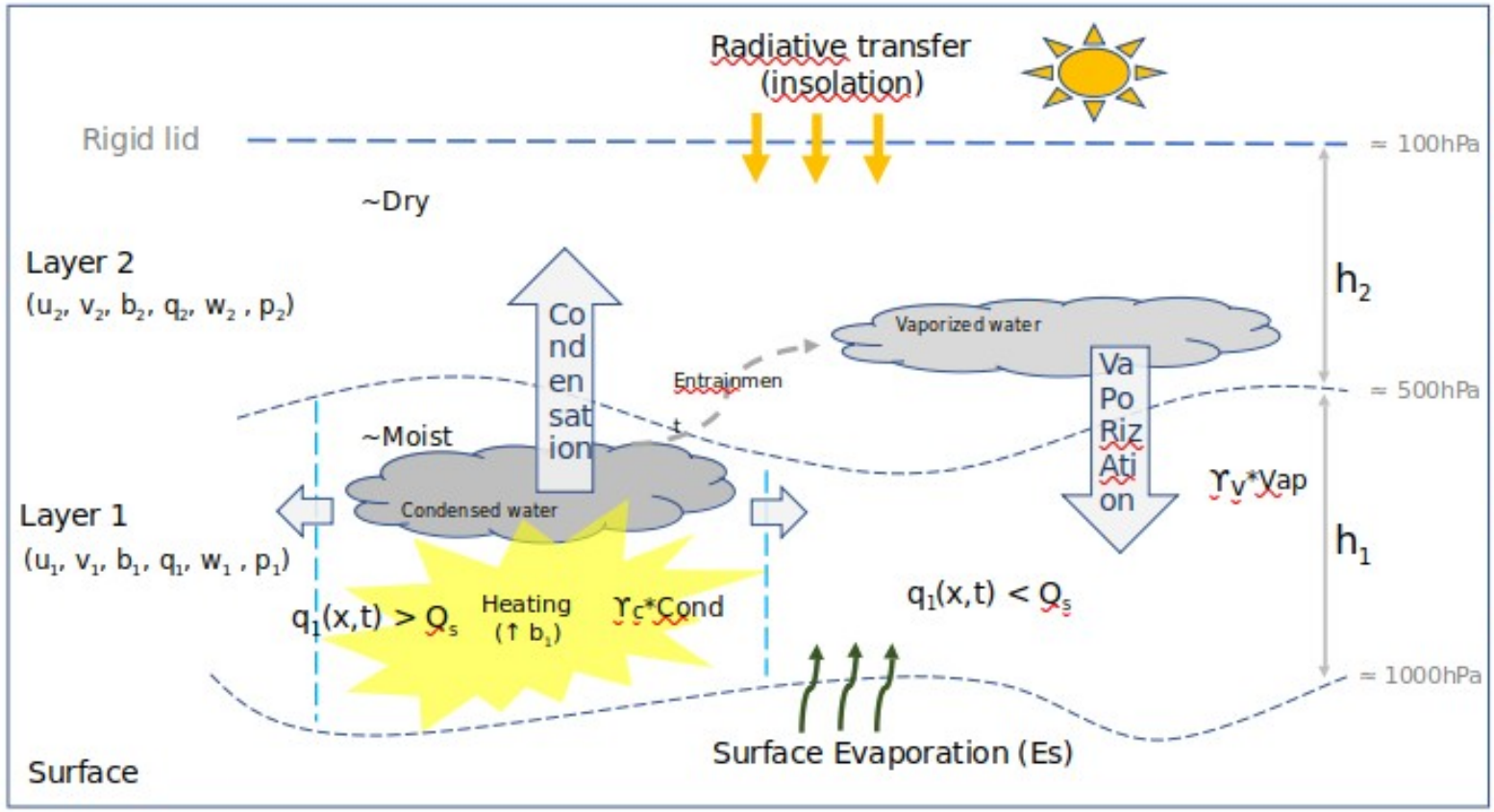

Where:

- Vap = vaporization
- Cond = condensation
- Υ_c * Cond = Entrainment

- u,v = velocity wind
- b = buoyancy
- q = water vapor
- w = precipitable water
- p = precipitation
- Es = surface evaporation

- h = layer thickness

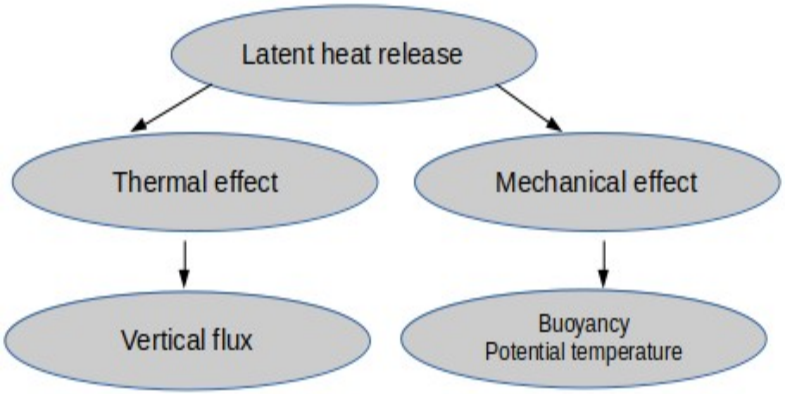

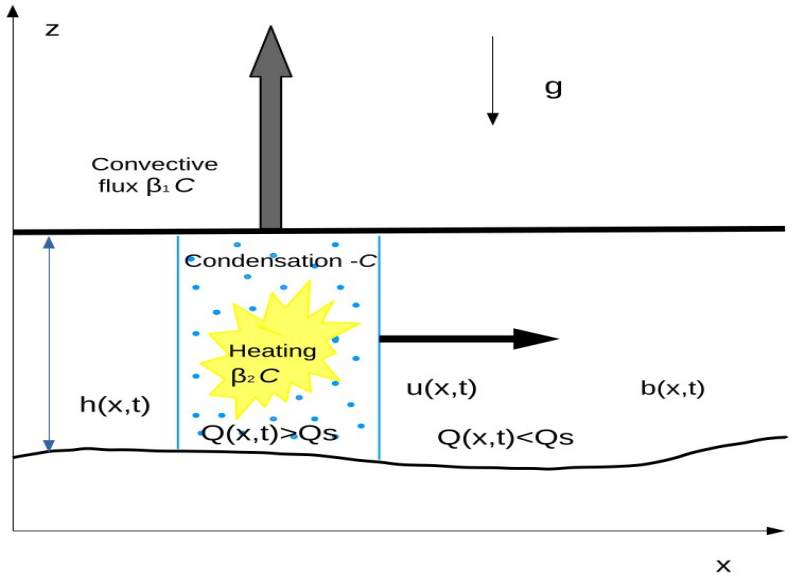

We can divide the influence of the latent heat release into two parts:

1) heating, that leads to local increase of buoyancy,

2) *convective flux*.

What are the improvements made to the moist-convective scheme?

$$
\begin{aligned}
(\partial_t + \boldsymbol{v}_1 \cdot \boldsymbol{\nabla})\boldsymbol{v}_1 + f\hat{\boldsymbol{z}} \times \boldsymbol{v}_1 &= -\langle \boldsymbol{\nabla} p_1 \rangle, \\
(\partial_t + \boldsymbol{v}_2 \cdot \boldsymbol{\nabla})\boldsymbol{v}_2 + f\hat{\boldsymbol{z}} \times \boldsymbol{v}_2 &= -\langle \boldsymbol{\nabla} p_2 \rangle - \frac{1-\gamma}{b_2 h_2}(\boldsymbol{v}_2 - \boldsymbol{v}_1)\,(\mathcal{C} - \mathcal{D}), \\
\partial_t h_1 + \boldsymbol{\nabla} \cdot (h_1 \boldsymbol{v}_1) &= \frac{1}{b_1}\left[(1-\gamma)(-\mathcal{C} + \mathcal{D}) - (1-\gamma^{\mathbb{F}})\,\mathbb{F}_1\right], \\
\partial_t h_2 + \boldsymbol{\nabla} \cdot (h_2 \boldsymbol{v}_2) &= \frac{1}{b_2}\left[(1-\gamma)(+\mathcal{C} - \mathcal{D}) - (1-\gamma^{\mathbb{F}})\,\mathbb{F}_2\right], \\
\partial_t b_1 + \boldsymbol{v}_1 \cdot \boldsymbol{\nabla}\, b_1 &= \frac{1}{h_1}\left[(+\mathcal{C} - \mathcal{D}) + \mathbb{F}_1\right], \\
\partial_t b_2 + \boldsymbol{v}_2 \cdot \boldsymbol{\nabla}\, b_2 &= \frac{1}{h_2}\left[(-\mathcal{C} + \mathcal{D}) + \mathbb{F}_2\right], \\
\partial_t q_1 + \boldsymbol{\nabla} \cdot (q_1 \boldsymbol{v}_1) &= -\mathcal{C} + \mathcal{D}^*, \\
\partial_t q_2 + \boldsymbol{\nabla} \cdot (q_2 \boldsymbol{v}_1) &= +\mathcal{C} - \mathcal{D}.
\end{aligned}
$$

Adiabatic convective

Diabatic non-convective

$$\int_{\mathcal{D}} \sigma \mathcal{C}\, d^2x = \int_{\mathcal{D}} (1-\sigma)\mathcal{D}\, d^2x,$$

convective updrafts = downdrafts in non-condensing regions

Precipitable water:

$$\partial_t W_i + \boldsymbol{\nabla} \cdot (W_i \boldsymbol{v}_i) = +\mathcal{C}_i - V_i.$$

Precipitation:

$$\mathcal{P} = \frac{W_1 - W_{cr}}{\tau_p} \mathcal{H}(W_1 - W_{cr}).$$

We establish equivalence between the spatial integration of sea surface evaporation, denoted by S_{vapor} , and the corresponding depletion term (D) in the upper layer.

$$\int \int_{\mathcal{D}} (\mathcal{S}_{\text{vapor}} = \mathcal{D}^*)\, d^2x\, dt \approx \int \int_{\mathcal{D}} \mathcal{D}\, d^2x\, dt.$$

Hamiltonian Structure of the model for conservation laws

If a system is Hamiltonian, then the evolution equations governing the field variables φ^a can be expressed utilizing the generalized Hamiltonian structures as follows:

$$\partial_t \varphi^a = \{\varphi^a, \mathcal{H}\} = \mathbb{J}^{ab} \frac{\delta \mathcal{H}}{\delta \varphi^b}. \quad (\varphi) = (u_1, v_1, h_1, b_1, u_2, v_2, h_2, b_2)^T \text{ is the phase space.}$$

H represents the Hamiltonian, and J denotes the Poisson tensor.

Hamiltonian = total energy

$$\mathcal{H} = \int_{\mathcal{D}} d^2x \left[h_1 \left(\frac{1}{2} \boldsymbol{v}_1^2 + \tilde{h_1} b_1 \right) + h_2 \left(\frac{1}{2} \boldsymbol{v}_2^2 + \tilde{h_2} b_2 \right) \right].$$

The functional derivatives of the Hamiltonian H are:

$$\frac{\delta \mathcal{H}}{\delta \boldsymbol{v}_k} = h_k \boldsymbol{v}_k, \quad \frac{\delta \mathcal{H}}{\delta h_k} = \zeta_k, \quad \frac{\delta \mathcal{H}}{\delta b_k} = h_k \tilde{h_k}.$$

The model may be written in non-canonical Hamiltonian form as: $\partial_t(\varphi) = \mathbb{J}\begin{pmatrix}\mathbb{M}_1\\ \mathbb{M}_2\end{pmatrix}$,

$(\varphi) = (u_1, v_1, h_1, b_1, u_2, v_2, h_2, b_2)^T$: The phase space

and the matrices $\mathbb{M}_i$ are defined as follows:

$$\mathbb{J} = \begin{pmatrix}\mathbb{J}_1 & \mathbb{O}\\ \mathbb{O} & \mathbb{J}_2\end{pmatrix}, \quad \mathbb{J}_i = \begin{pmatrix} 0 & \mathbb{Q}_i & -\partial_x & h_i^{-1}\partial_x b_i \\ -\mathbb{Q}_i & 0 & -\partial_y & h_i^{-1}\partial_y b_i \\ -\partial_x & -\partial_y & 0 & 0 \\ -h_i^{-1}\partial_x b_i & -h_i^{-1}\partial_y b_i & 0 & 0 \end{pmatrix}, \quad i = 1, 2,$$

$$\mathbb{M}_i = \begin{pmatrix} h_i u_i \\ h_i v_i \\ \zeta_i \\ h_i \tilde{h}_i \end{pmatrix}, \quad i = 1, 2.$$

$\zeta_i = \tilde{p}_i + (1/2)\boldsymbol{v_i^2}$ represents the Bernoulli head in each layer.

The potential vorticity:

$$\partial_t \mathbb{Q}_i + \boldsymbol{v}_i \cdot \boldsymbol{\nabla} \mathbb{Q}_i = h_i^{-1} J(\tilde{h}_i, b_i), \quad i = 1, 2,$$

$J(f, g) = \partial_x f \partial_y g - \partial_y f \partial_x g$ is the Jacobian of the two functions.

Hyperbolicity criterion:

$$(v_1 - v_2)^2 \leq \left(1 - \frac{b_1}{b_2}\right)(h_1 b_1 + h_2 b_2),$$

loss of hyperbolicity = emergence of Kelvin-Helmholtz type instabilities

Numerical method of Aeolus2.0:
spin-weighted spherical harmonics

General basis vectors **vs.** spin-weighted set of basis vectors

Orthonormal coordinate unit vectors

$$\nabla_\theta f(\theta,\phi) = \frac{\partial}{\partial\theta} f(\theta,\phi), \quad \nabla_\phi f(\theta,\phi) = \frac{1}{\sin\theta}\frac{\partial}{\partial\phi} f(\theta,\phi).$$

$$\nabla = e_\theta \nabla_\theta + e_\phi \nabla_\phi,$$

$$\nabla e_\theta = \cot\theta\, e_\phi e_\phi, \quad \nabla e_\phi = -\cot\theta\, e_\phi e_\theta.$$

$$e_\pm = \frac{1}{\sqrt{2}}(e_\theta \mp i e_\phi).$$

$$\nabla e_\pm = \pm i \cot\theta e_\phi e_\pm = \pm\frac{\cot\theta}{\sqrt{2}}(e_- - e_+)e_\pm.$$

$$\nabla \equiv e_\mu \nabla_\mu = e_+\nabla_+ + e_-\nabla_-,$$

$$\nabla_\pm = \frac{1}{\sqrt{2}}\left(\nabla_\theta \pm i\nabla_\phi\right).$$

The spin basis vectors + spin-weighted spherical harmonics → A very simple action for the ***'regular' gradient operator:*** getting rid of the singular nature of the basis vectors at the poles. Gradient = diagonal wavenumber multiplication that remains regular everywhere

Spin-weighted spherical harmonics:

$$Y^s_{l,m}$$

Spin basis:

$$e_{\pm 1} = e_\theta \mp i e_\phi$$

$$T = \sum_{l,m,\sigma} T^\sigma_{l,m} Y^{\bar\sigma}_{l,m} e_\sigma \qquad \sigma \in \{\pm 1\}^N$$

Spin gradient:

$$\nabla^\mu (Y^{\bar\sigma}_{l,m} e_\sigma) = k_l^{\bar\sigma,\mu} Y^{\bar\sigma+\mu}_{l,m} e_\sigma \qquad \mu \in \{\pm 1\}$$

$$\nabla^\mu T \to k_l^{\bar\sigma,\mu} T^\sigma_{l,m}$$

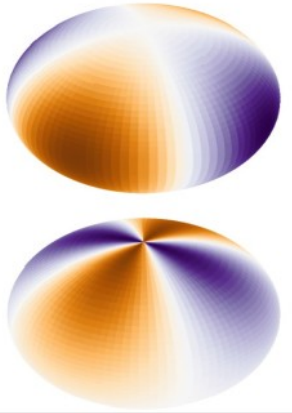

Numerical method of Aeolus2.0

Initial value problems - the LHS coefficients are time independent, the LHS is first order in time derivatives, and the RHS has no time derivatives:

$$\mathcal{M} \cdot \partial_t \mathcal{X} + \mathcal{L} \cdot \mathcal{X} = \mathcal{F}(\mathcal{X}, t).$$

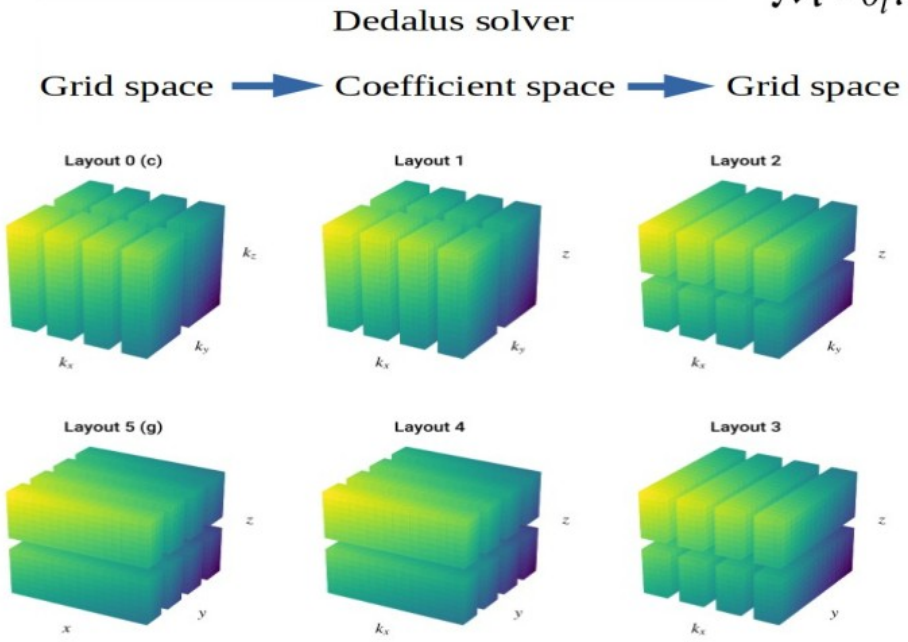

The transforms (TF) and transpositions (TP) stepping between layouts are indicated.
Sparse solver: a subset of the eigenmodes near a specified target eigenvalue

Some distinguished features of Aeolus2.0:

Front resolving feature of Aeolus2.0

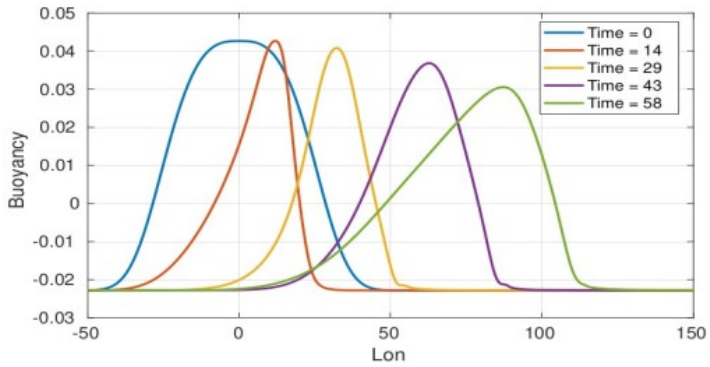

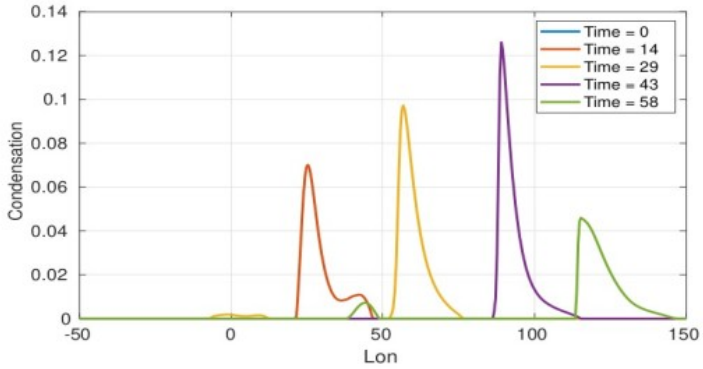

Different collocation grids for the implemented bases.

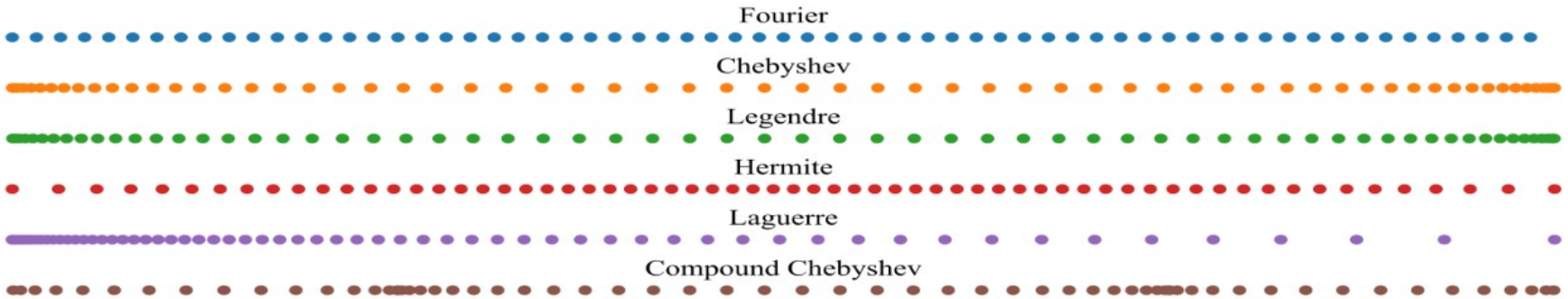

Dynamical core:
Pseudo spectral moist-convective Thermal Rotating Shallow Water (mcTRSW) model

Water cycle + Boundary Layer

Moist-convection (updraft - downdraft)

Bottom topography

Insolation + Rapid Radiative Transfer Model (RRTM),
[water vapor, carbon dioxide, ozone, methane, nitrous oxide, and the common halocarbons]

Dedalus solver

Grid space → Coefficient space → Grid space

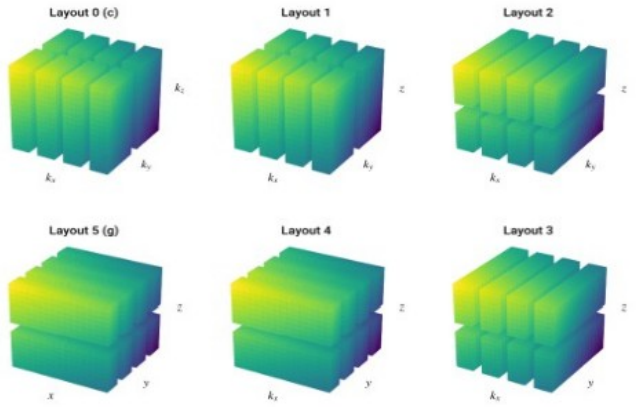

Spin-weighted spherical harmonics:

$$Y^s_{l,m}$$

Spin basis:

$$e_{\pm 1} = e_\theta \mp i e_\phi$$

$$T = \sum_{l,m,\sigma} T^\sigma_{l,m} Y^\sigma_{l,m} e_\sigma \qquad \sigma \in \{\pm 1\}^N$$

Spin gradient:

$$\nabla^\mu (Y^{\bar{\sigma}}_{l,m} e_\sigma) = k_l^{\bar{\sigma},\mu} Y^{\bar{\sigma}+\mu}_{l,m} e_\sigma \qquad \mu \in \{\pm 1\}$$

$$\nabla^\mu T \to k_l^{\bar{\sigma},\mu} T^\sigma_{l,m}$$

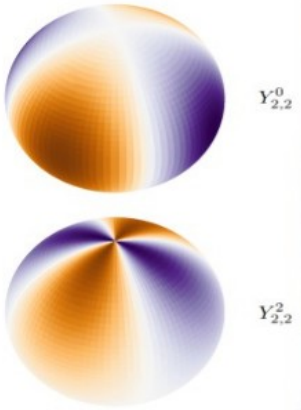

Some distinguished/existing features of Aeolus2.0:

Capturing heat fluxes and extremes

1) To get rid of the singular nature of the classical basis vectors at the poles: ***regular gradient operator***.
2) ***Robust dynamical core*** over the whole sphere with layers interaction.
3) Possibility of ***high resolution with high running speed***.
4) Possibility of nudging ***non-equidistant grid system*** for desired region.
5) Utilizing advanced version of ***Rapid Radiative Transfer Model (RRTM)*** by treating more than 10 molecular species over 16 contiguous bands.
6) Possibility of using ***a hierarchy level of complexities*** to find out the trace of causality easily.
7) The model is self-consistent and also has consistent and physically ***reasonable asymptotic limits***. Converged solution toward eigenvalue solution.
8) Capturing the ***convection-coupled gravity and equatorial waves.***
9) The model uses ***minimal parametrization***, most parameters are independent of numerical resolution.
10) Investigating ***energy flux*** by means of pseudo-energy density in mcTRSW satisfies the local conservation of energy flux.

$$E_P = \frac{1}{2}h|\boldsymbol{u}|^2 + \frac{1}{2}\left(\sqrt{\Theta}h - \sqrt{\Theta_0}H_0\right)^2,$$

11) Capturing full ***non-linearity of large-scale and synoptic scale*** flows.

Application of Aeolus 2.0:
On the genesis and dynamics of MJO-like structure by equatorial adjustment of localized heating

Potsdam Institute for Climate Impact Research

What is the MJO?

The Madden-Julian Oscillation (MJO) is the dominant slowly eastward propagating mode of intra-seasonal planetary scale variability in the tropical atmosphere.

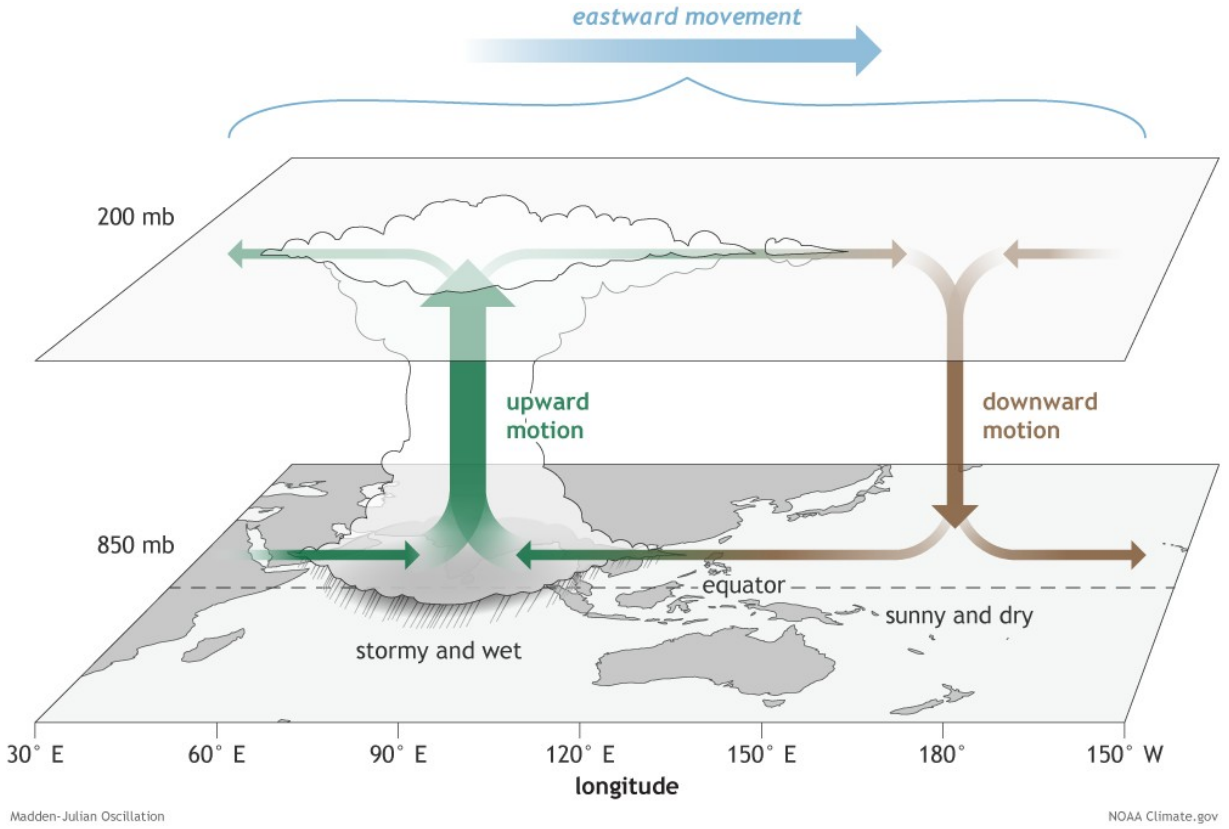

Main features of the MJO:

The periodically arising ***large-scale*** patterns of enhanced ***deep convection*** which are ***slowly moving eastward*** from the Indian Ocean over the maritime continent and are ***dying out*** in the Pacific.

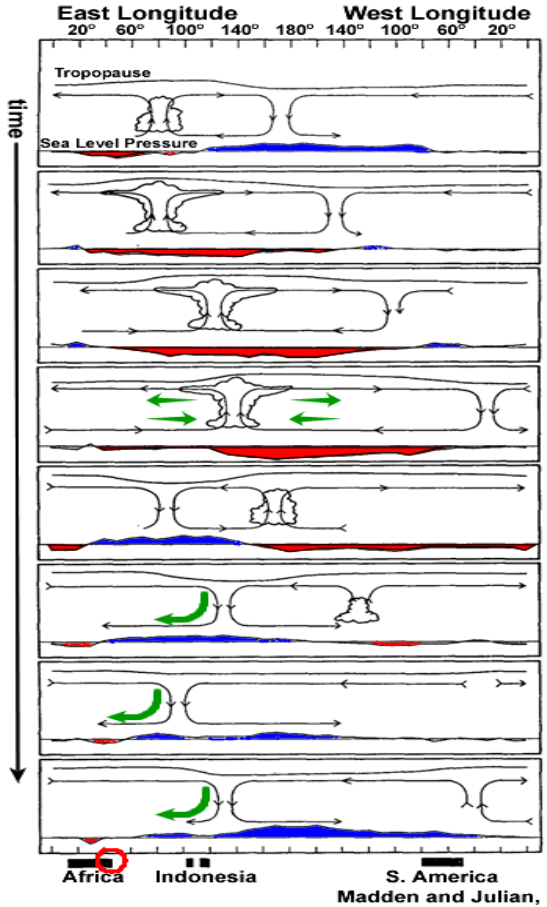

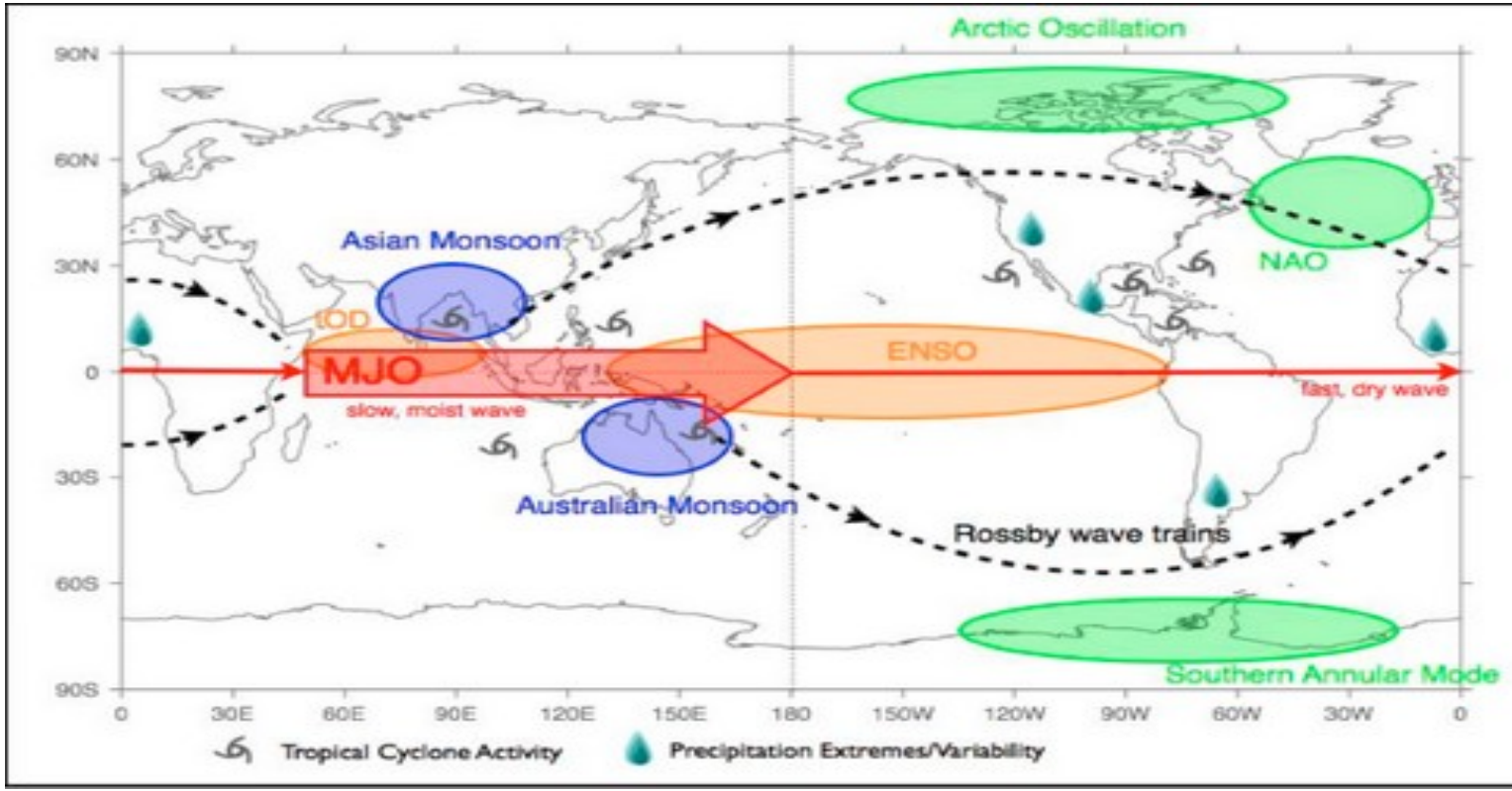

Our theory

Genesis theory: MJO-like structure can be generated in a self-sustained and self-propelled manner due to nonlinear relaxation (adjustment) of a large-scale positive buoyancy anomaly, depressed anomaly, or a combination of them, as soon as this anomaly reaches a critical threshold in the presence of moist-convection at the equator.

How this condition can be provided? Interaction of the Baroclinic Kelvin wave (BKW), after circumnavigating all around the equator, with a new large-scale buoyancy anomaly may contribute to excitation of a recurrent generation of the next cycle of MJO-like structure.

Hybrid Structure: it consists of a “quasi equatorial modon”, with an enhanced vortex pair, and a convectively coupled baroclinic Kelvin wave (BKW), with greater phase speed than that of modon on the intraseasonal time scale.

What is Equatorial Modon?

An exact, form-preserving, eastward uniformly translating, horizontally localized, nonlinear solution to the inviscid quasi-geostrophic equations (Rostami & Zeitlin, 2019a).

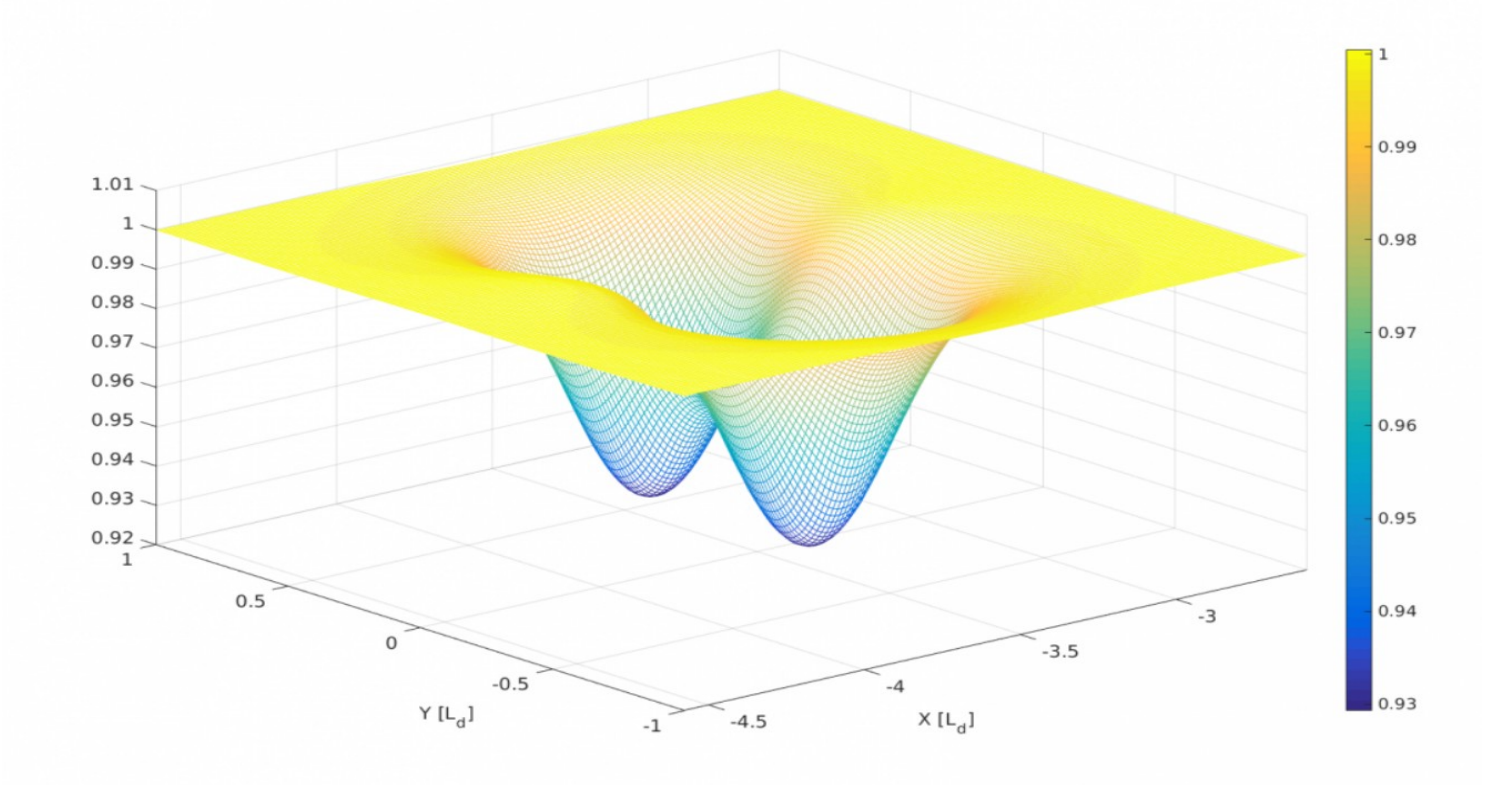

Asymptotic solutions

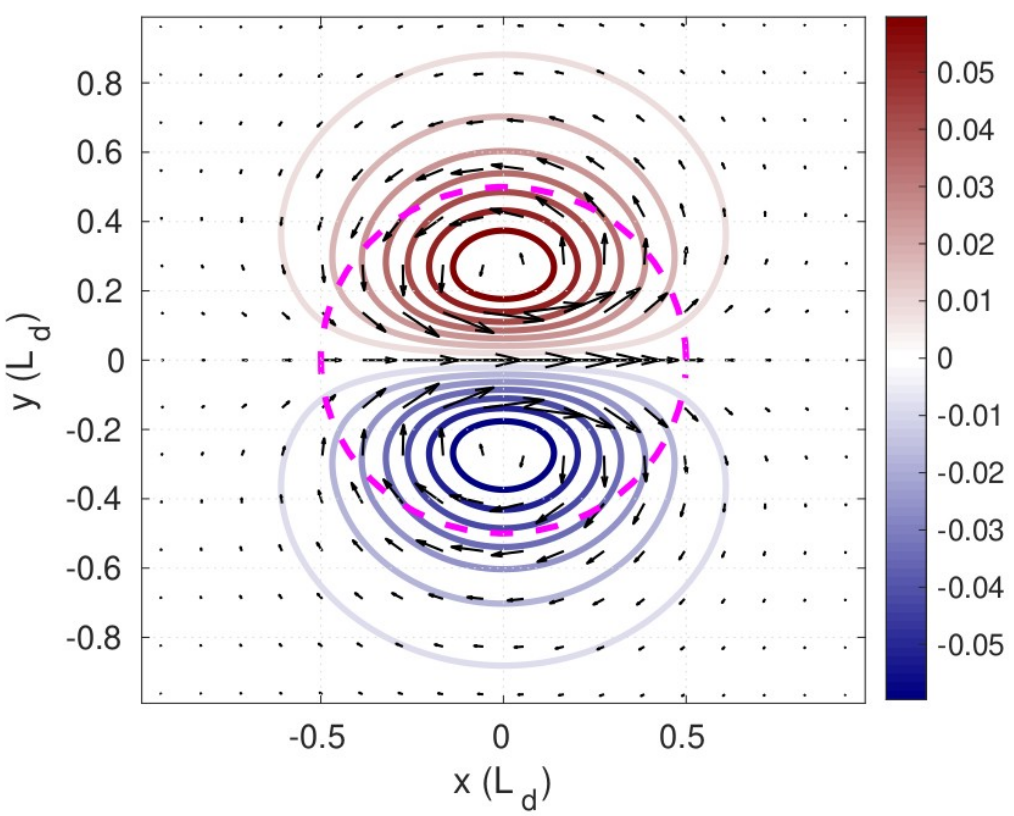

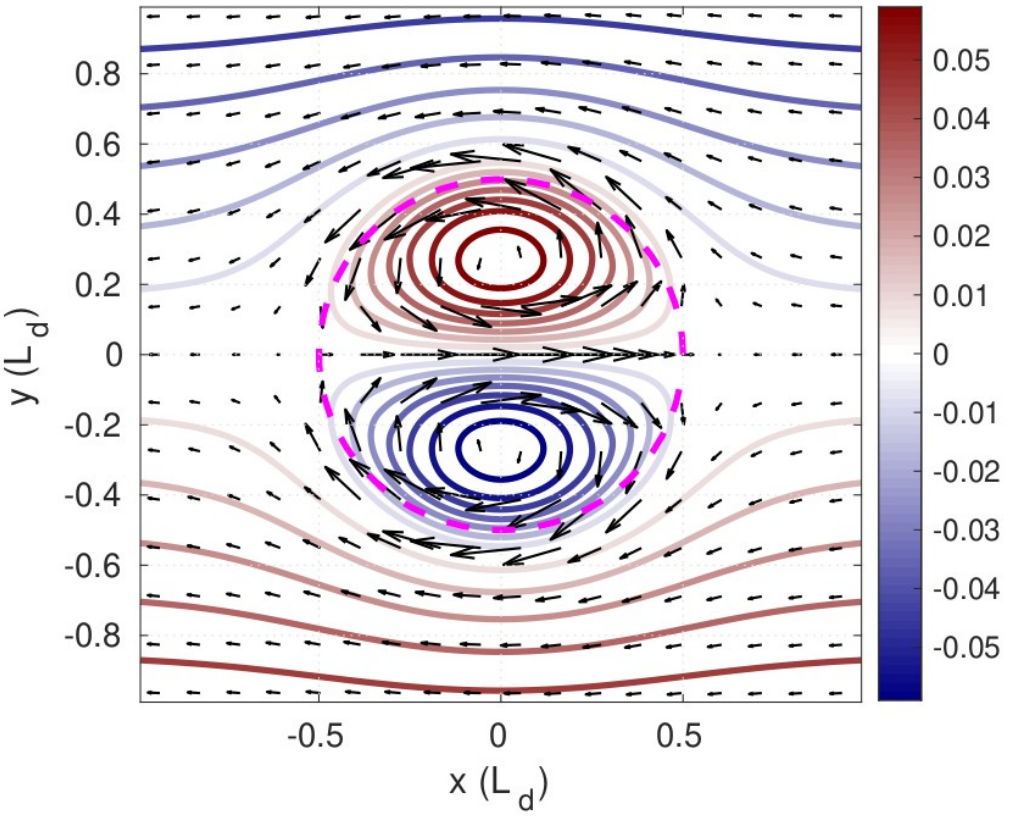

Streamlines and velocity field of an asymptotic modon in stationary (left) and co-moving (right) frames with U = 0.1 . Dashed circle: separatrix of radius a = 0.5 .

Conversion of asymptotic modon to “adjusted modon” in a self sustained manner

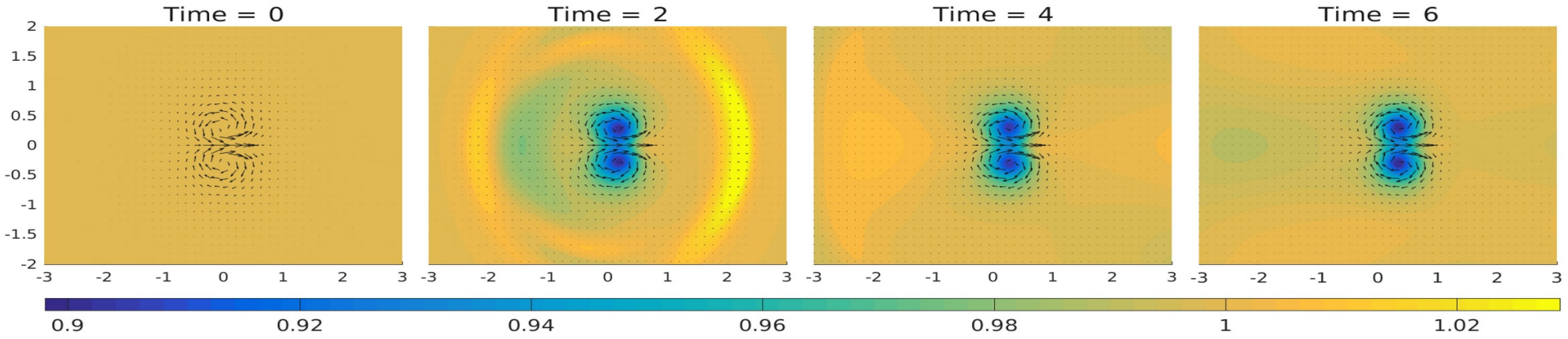

Emerging of “adjusted” EM from asymptotic modon under Charney regime.

Asymptotic solution of EM:

$$\begin{cases} \psi_{ext} = -\frac{Ua}{K_1(pa)} K_1(pr)\sin\theta,\ p^2 = \overline{\beta}/U,\ U>0, \quad r>a, \\ \psi_{int} = \left[\frac{Up^2}{k^2 J_1(ka)} J_1(kr) - \frac{r}{k^2}(1+U+Uk^2)\right]\sin\theta, \quad r<a, \end{cases}$$

J_1 and K_1 are ordinary and modified Bessel functions of order one.

Theory: Charney regime in Equatorial RSW

RSW equations

$$\begin{cases} \partial_t \mathbf{v} + \mathbf{v}\cdot\nabla\mathbf{v} + \beta\, y\, \hat{\mathbf{z}}\wedge\mathbf{v} + g\nabla h = 0\,, \\ \partial_t h + \nabla\cdot(\mathbf{v}h) = 0\,, \end{cases} \tag{1}$$

Scaling $h = H(1+\lambda\eta)$, $(x,y)\sim L$, $(u,v)\sim V$, $t\sim L/V$, $\overline{\beta} = \beta L^2/V$. If $gH\lambda/V^2 = \mathcal{O}(1) \Rightarrow V << \sqrt{gH}$:

$$\partial_t \mathbf{v} + \mathbf{v}\cdot\nabla\mathbf{v} + \overline{\beta}\, y\, \hat{\mathbf{z}}\wedge\mathbf{v} + \nabla\eta = 0\,, \tag{2}$$

$$\lambda(\partial_t\eta + \mathbf{v}\cdot\nabla\eta) + (1+\lambda\eta)\,\nabla\cdot\mathbf{v} = 0, \tag{3}$$

Leading order in $\lambda \Rightarrow \nabla\cdot\mathbf{v}_0 = 0 \Rightarrow u_0 = -\partial_y\psi,\ v_0 = \partial_x\psi$,

$$\nabla^2\psi_t + \mathcal{J}(\psi, \nabla^2\psi) + \overline{\beta}\psi_x = 0, \quad \mathcal{J} - \text{Jacobian}. \tag{4}$$

Asymptotic solutions

Steady modon (Rostami & Zeitlin, 2019) with zonal velocity U:

$$\begin{cases} \psi_{ext} = -\frac{Ua}{K_1(pa)} K_1(pr)\sin\theta,\ p^2 = \overline{\beta}/U,\ U > 0, \quad r > a, \\ \\ \psi_{int} = \left[\frac{Up^2}{k^2 J_1(ka)} J_1(kr) - \frac{r}{k^2}(1 + U + Uk^2)\right]\sin\theta, \quad r < a, \end{cases} \tag{5}$$

– J_1 and K_1 are ordinary and modified Bessel functions of order one.
– p is real, and $p^2 = \overline{\beta}/U$, so $U > 0$, and the motion is eastward.
– Each pair $(a, p) \rightarrow$ series of eigenvalues k arising from matching conditions, the lowest corresponds to a dipole.

Asymptotic solutions

Pressure distribution at a given ψ:

$$\nabla^2\eta = \mathit{Hess}[\psi] + \overline{\beta}(\psi_y + y\nabla^2\psi) \tag{6}$$

where $\mathit{Hess}[\psi] = \partial^2_{xx}\psi\partial^2_{yy}\psi - (\partial^2_{xy}\psi)^2$ is the Hessian operator. Note that equations 4 and 6 are shallow-water counterparts of the non-divergent model for large-scale tropical motions Charney (1963).

Phase portrait of “*asymptotic*” and “*adjusted*” Equatorial Modon (EM)

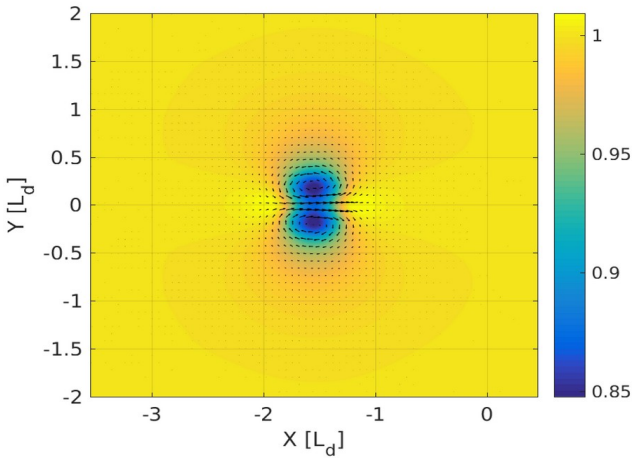

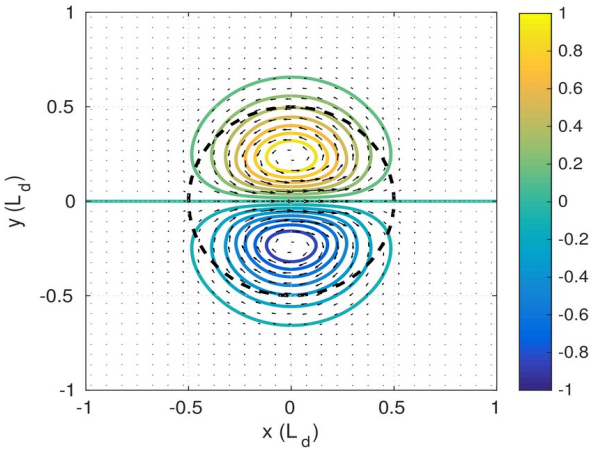

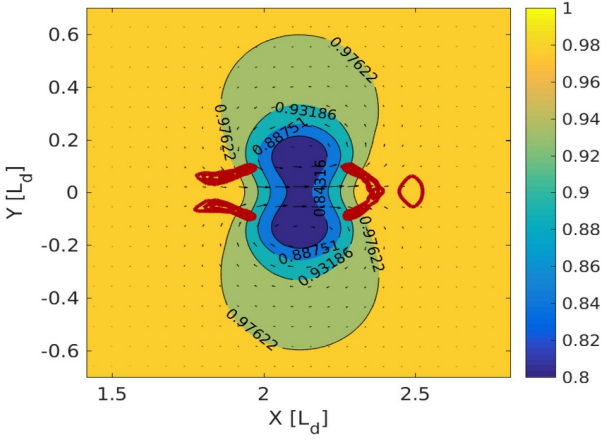

Left panel: Structure of the equatorial modon. Middle panel: Stream-function of the barotropic equatorial modon (asymptotic modon). Right panel: Convectively coupled equatorial modon showing the condensation regions. Dashed : separatrix r = a.

“Exact” vs asymptotic modon

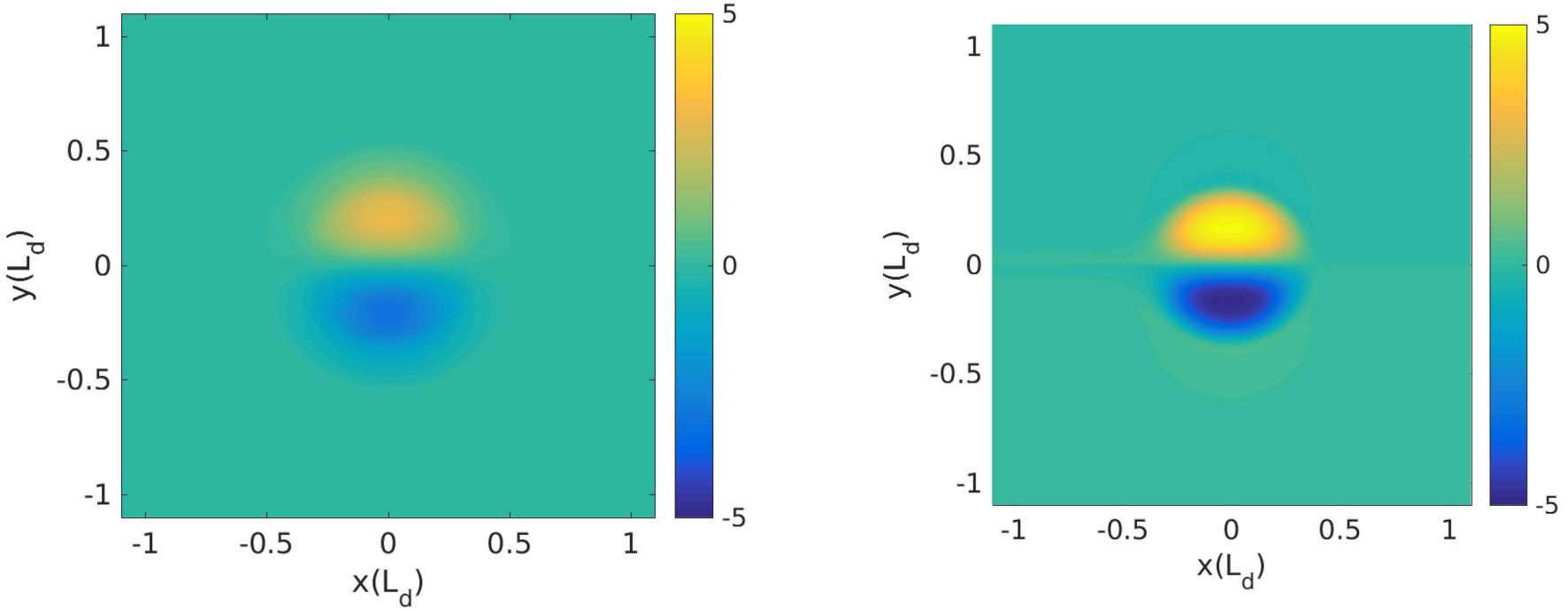

Relative vorticity of the asymptotic (left) vs “exact” (right) modons.

Coherence of the adjusted “true” modon

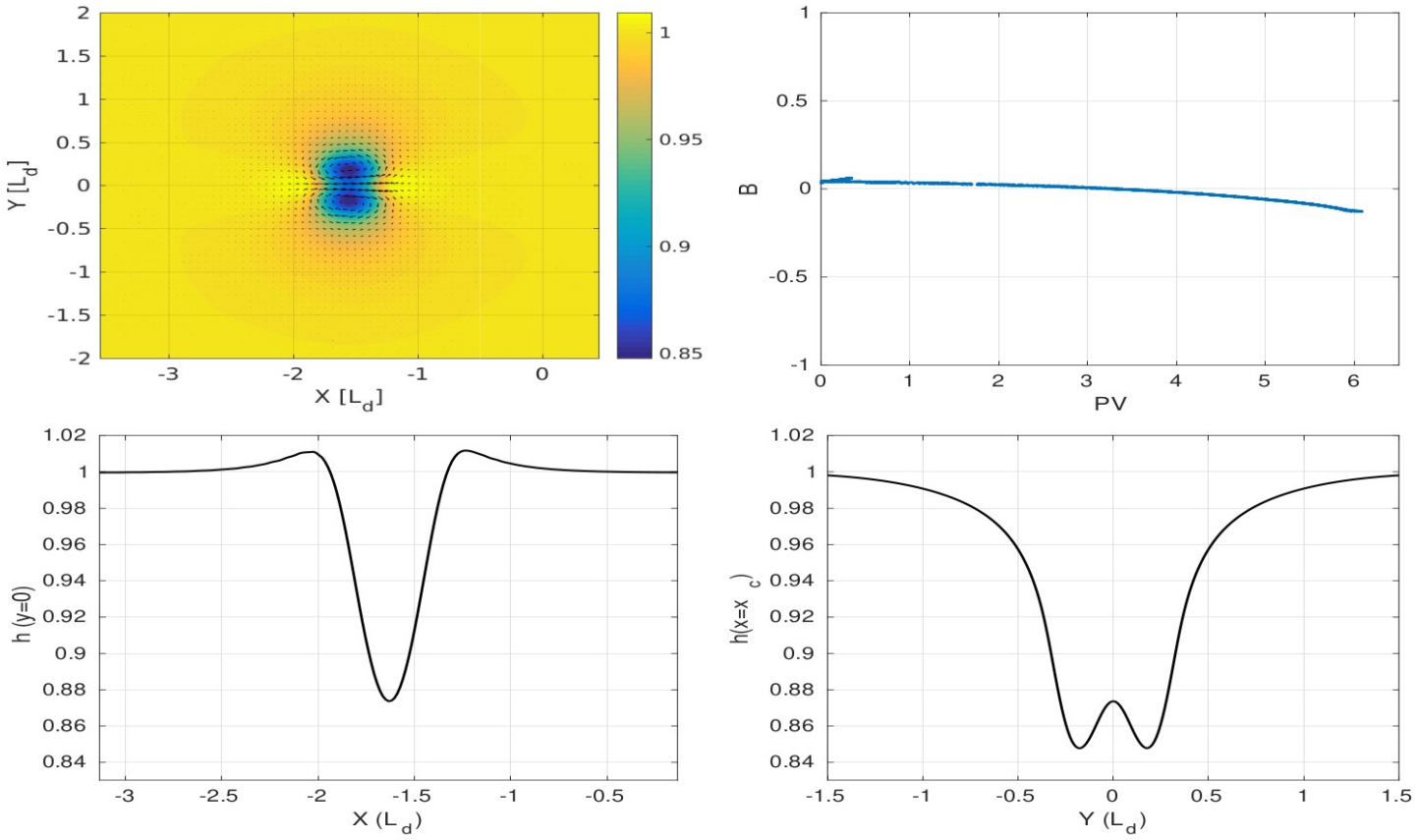

Thickness, Bernoulli function vs potential vorticity in the co-moving frame, zonal and meridional sections of the modon at t = 15 [1/βL d].

Evolution of the “true” modon

(pressure and div. fields)

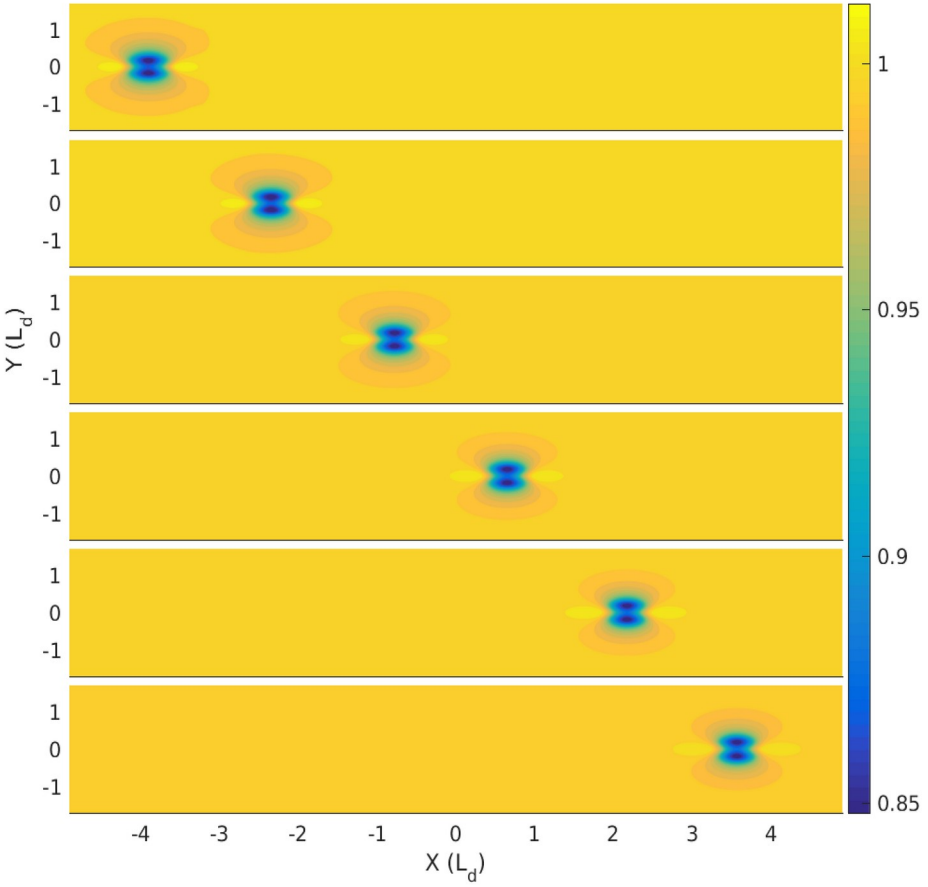

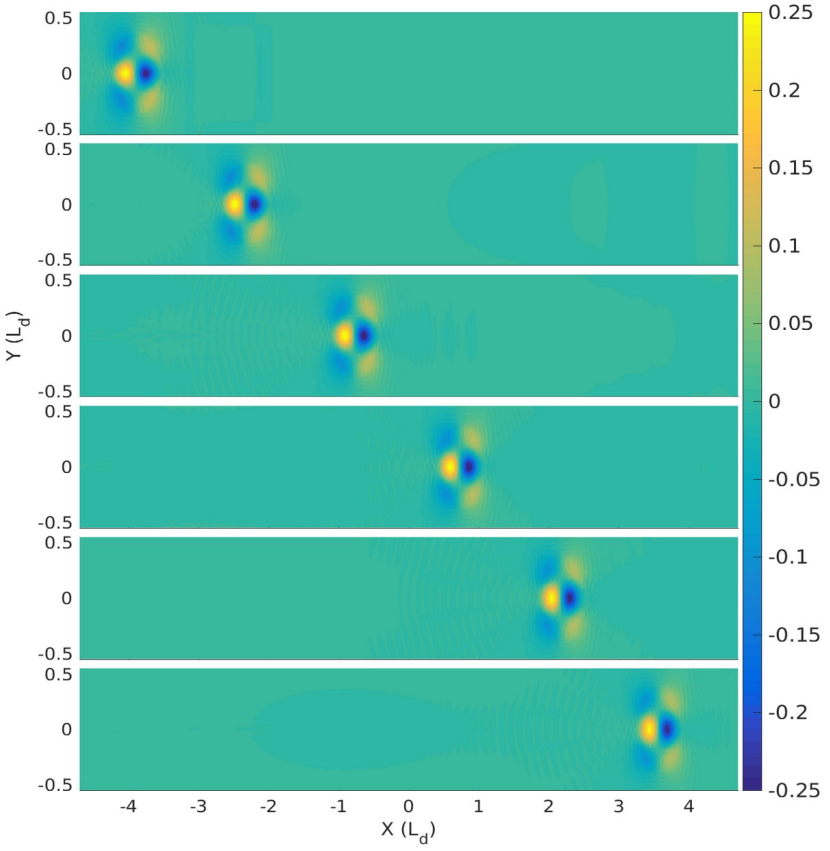

Eastward Propagation of Equatorial Modon in “dry” and its intensification in moist-convective environment

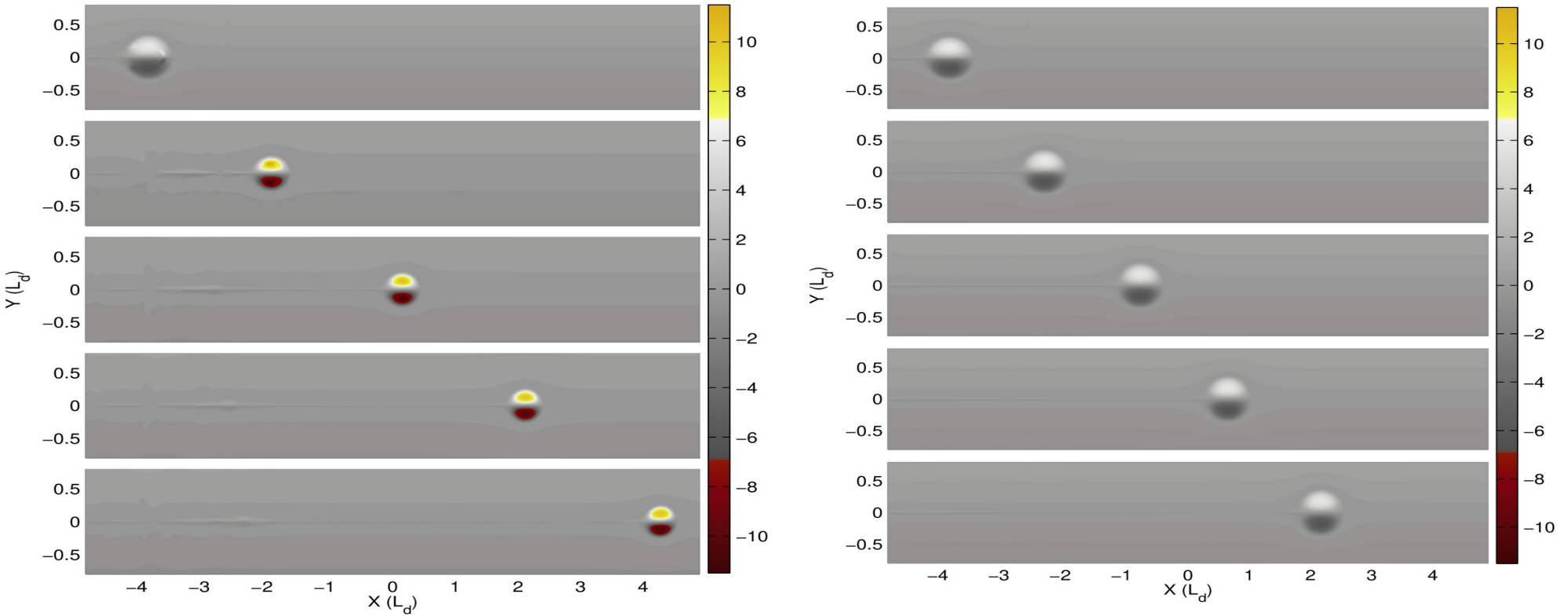

Steady eastward propagation of the equatorial modon, as seen in PV field in moist-convective (left) and adiabatic (right) environments.

Question: Can we generate a slowly eastward propagation in a self-sustained and self-propelling manner?

Answer: Yes, by geostrophic adjustment of large-scale localized heating (negative pressure or positive temperature anomaly) over the equator.

Question: This statement is against the well-known Gill's mechanism. Is Gill's mechanism non-universal?

Answer: Yes, ***Gill's mechanism is non-universal*** (Rostami and Zeitlin, 2019b).

What is Gill's mechanism?

Gill's mechanism of large-scale response to localized heating -folklore in tropical meteorology and climatology.

Quarterly Journal of the Royal Meteorological Society

RMetS

Quarterly Journal of the Royal Meteorological Society / Volume 106, Issue 449 / p. 447-462

Article

Some simple solutions for heat-induced tropical circulation

A. E. Gill

First published: July 1980

https://doi.org/10.1002/qj.49710644905

What is Gill's mechanism?

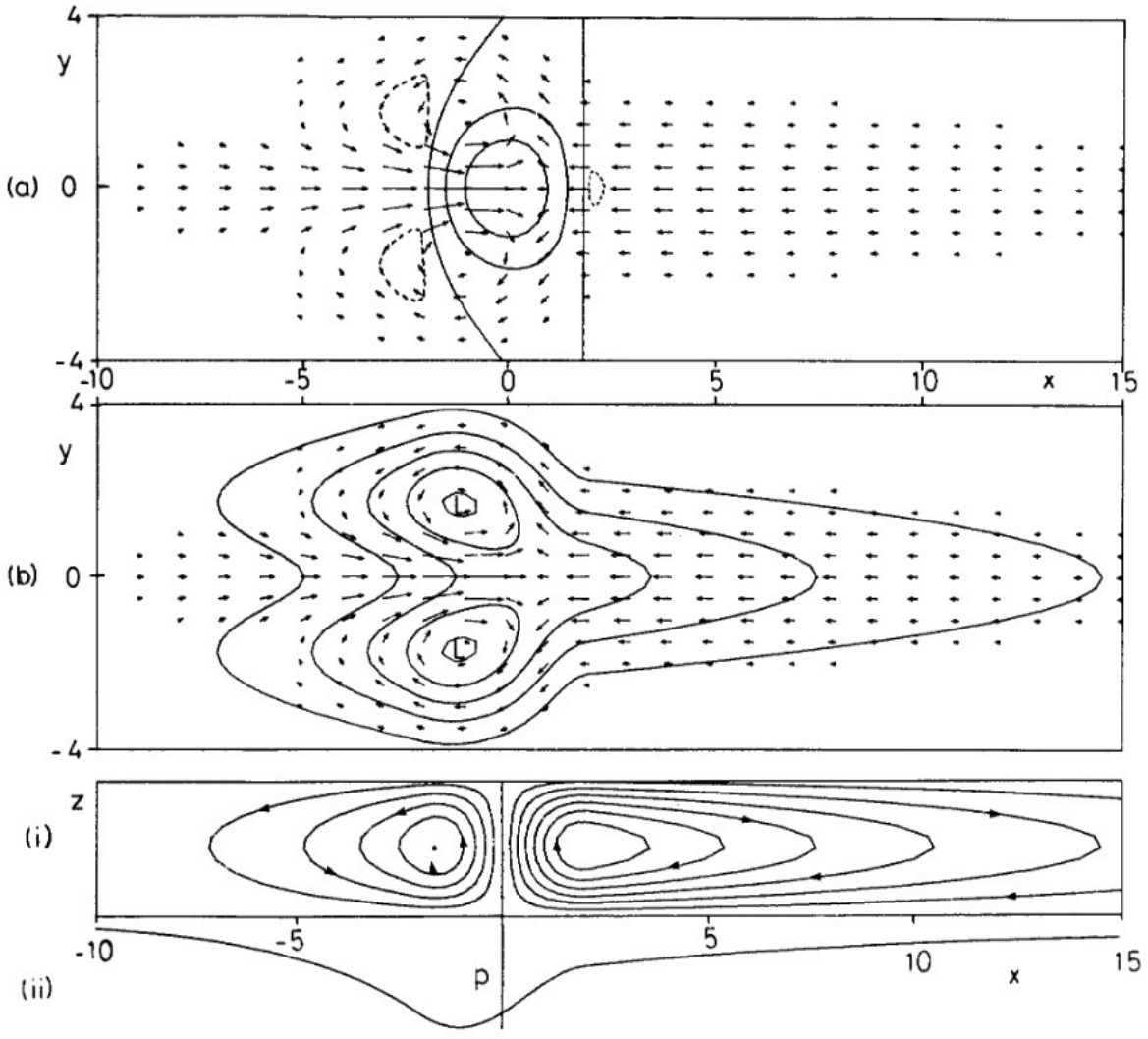

Figure 1. Solution for heating symmetric about the equator in the region $|x| < 2$ for decay factor $\varepsilon = 0{\cdot}1$.

(a) Contours of vertical velocity w (solid contours are 0, 0·3, 0·6, broken contour is −0·1) superimposed on the velocity field for the lower layer. The field is dominated by the upward motion in the heating region where it has approximately the same shape as the heating function. Elsewhere there is subsidence with the same pattern as the pressure field.

(b) Contours of perturbation pressure p (contour interval 0·3) which is everywhere negative. There is a trough at the equator in the easterly régime to the east of the forcing region. On the other hand, the pressure in the westerlies to the west of the forcing region, though depressed, is high relative to its value off the equator. Two cyclones are found on the north-west and south-west flanks of the forcing region.

(c) The meridionally integrated flow showing (i) stream function contours, and (ii) perturbation pressure. Note the rising motion in the heating region (where there is a trough) and subsidence elsewhere. The circulation in the right-hand (Walker) cell is five times that in each of the Hadley cells shown in (c).

Generation of Equatorial Modon from *Equatorial Excitable Systems* (EES)

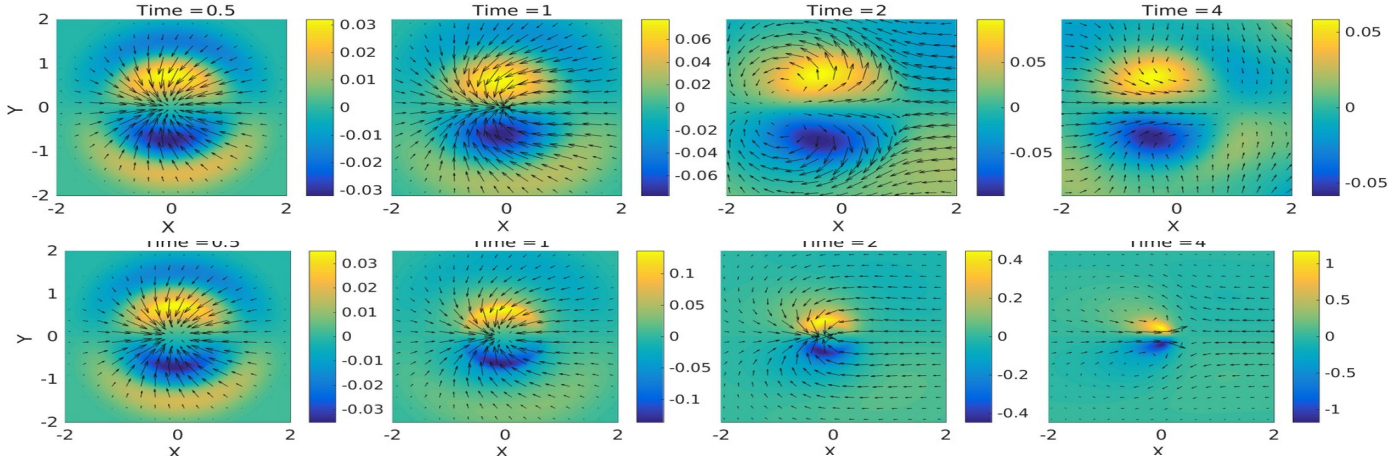

Fig. Snapshots of vorticity (colors) and velocity (arrows) of the initial stages of "dry" (top) and moist-convective, bottom) adjustments of a circular negative pressure anomaly with max $|\Delta H/H|$ = 0.1. Note a pronounced convergence at t = 2 $[1/\beta L_d]$ due to condensation in the bottom panel.

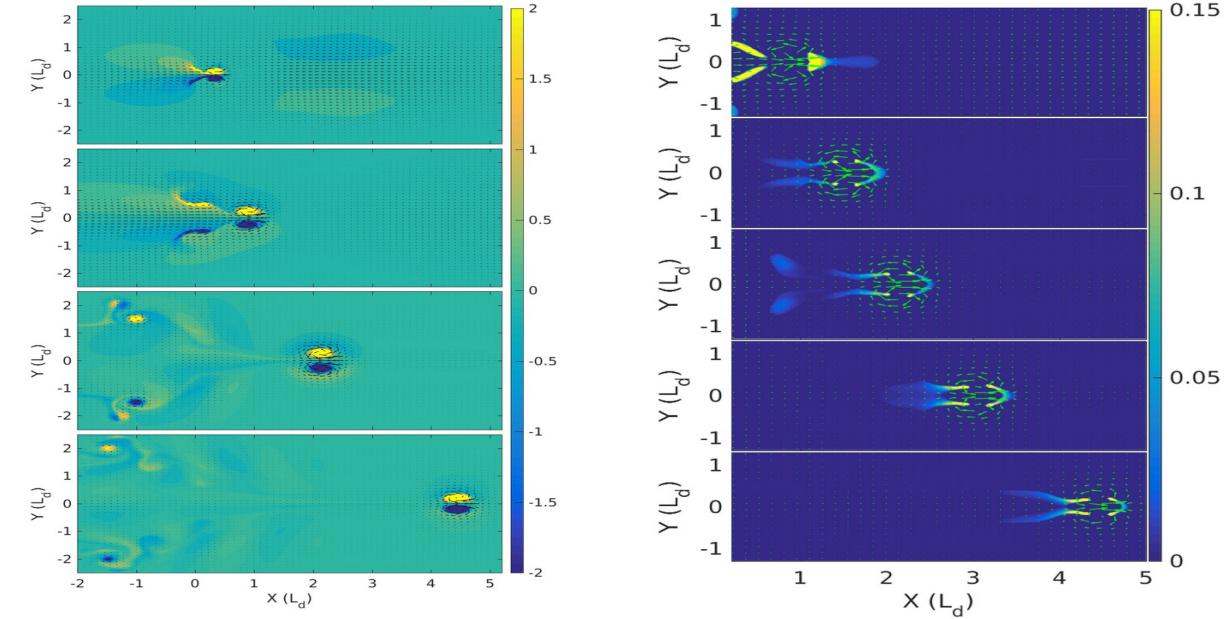

Fig. Evolution at later times t = 5, 30, 45, 75 $[1/\beta L_d]$ of relative vorticity during the moist-convective adjustment of circular negative pressure anomalies with max $|\Delta H/H|$ = 0.18 (left panel) and corresponding precipitation pattern.

Generation of MJO-like structure from geostrophic adjustment of baroclinic disturbances in tropical atmosphere (Rostami & Zeitlin, 2020)

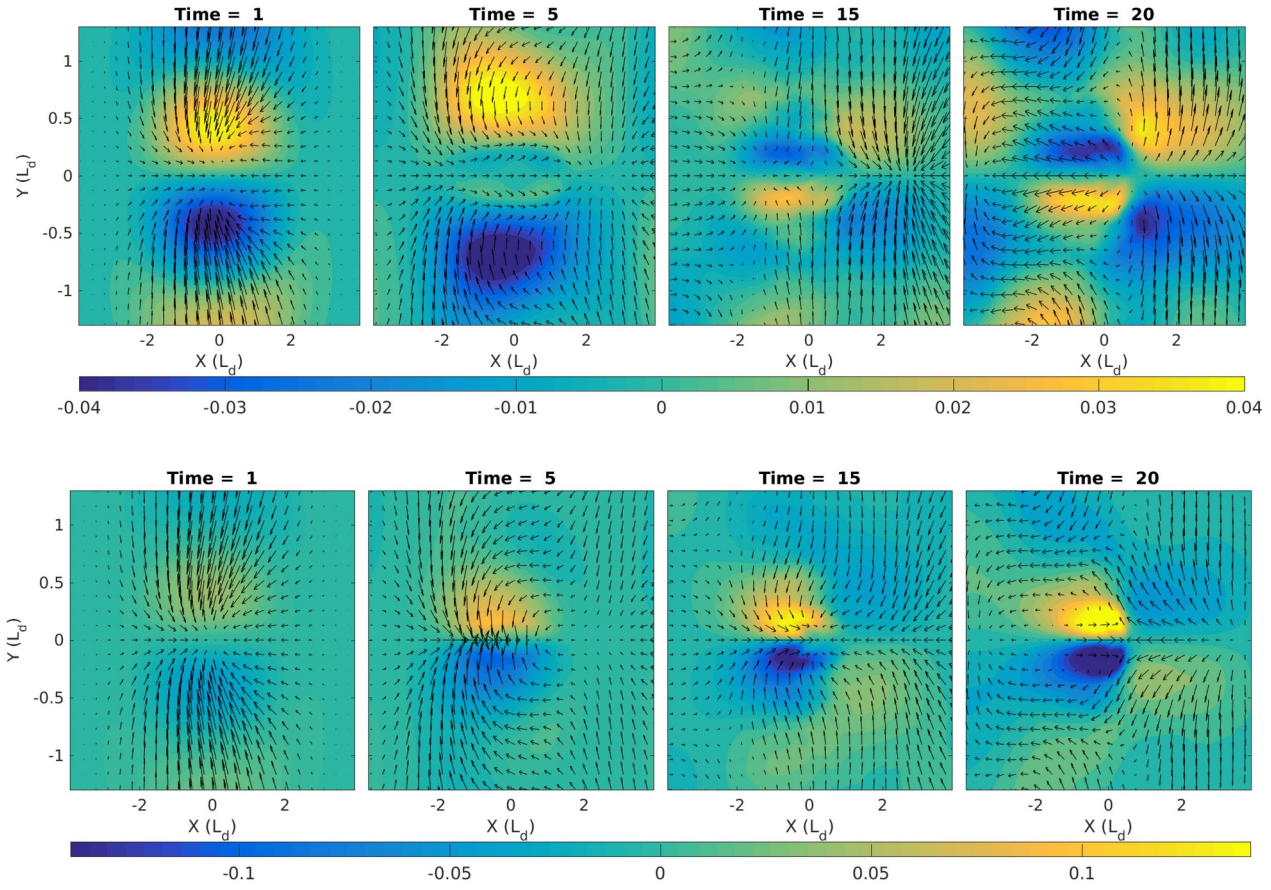

The initial evolution of velocity (arrows) and relative vorticity (colors) fields that correspond to the upper-layer and lower-layer components, respectively from top to bottom.

Hybrid structure: Baroclinic Modon-Kelvin Wave (initial stages)

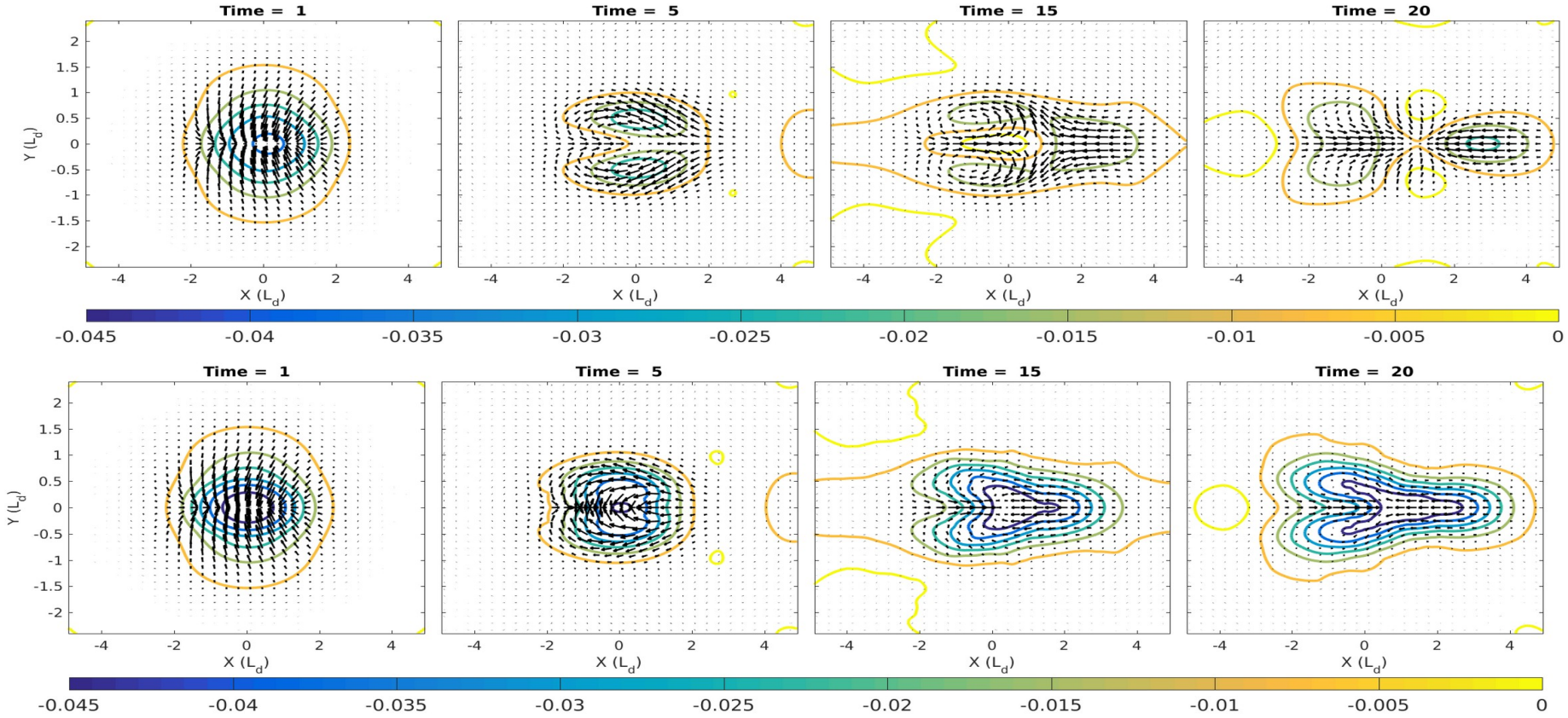

Initial stages of equatorial adjustment of a negative pressure anomaly in the lower layer as seen in evolution of the baroclinic velocity (arrows) and pressure anomaly (contours) in “dry” (upper panel) and moist-convective (lower panel) environments.

Hybrid structure: Baroclinic Modon-Kelvin Wave (late stages)

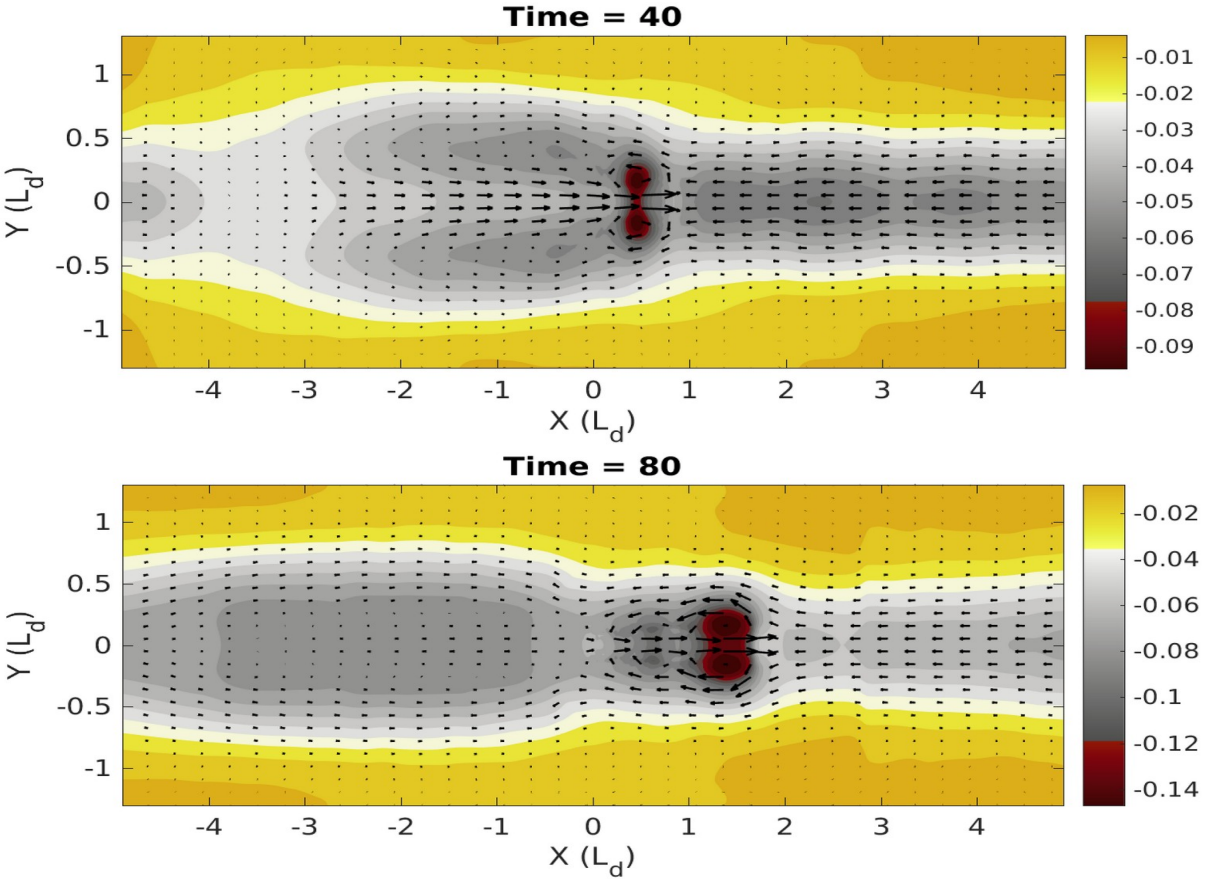

Eastward-propagating intense baroclinic dipole as seen in the baroclinic pressure anomaly (colors) and baroclinic velocity (arrows) at times t = 40, 80 $(L_d/\sqrt{gH_s})$.

Divergence and condensation patterns of hybrid structure

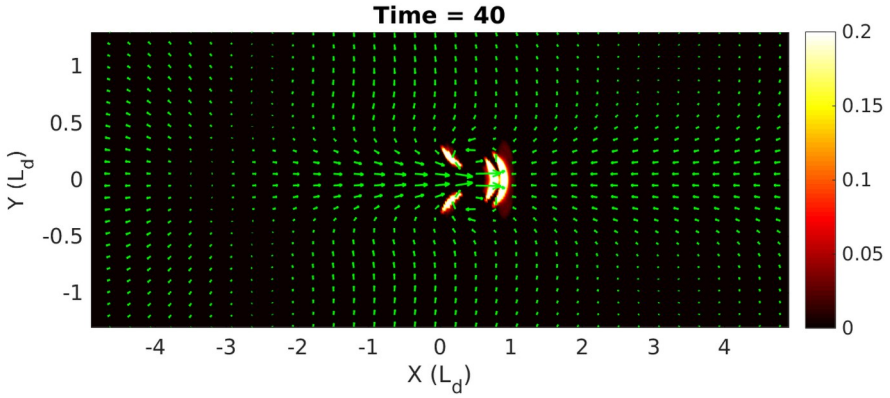

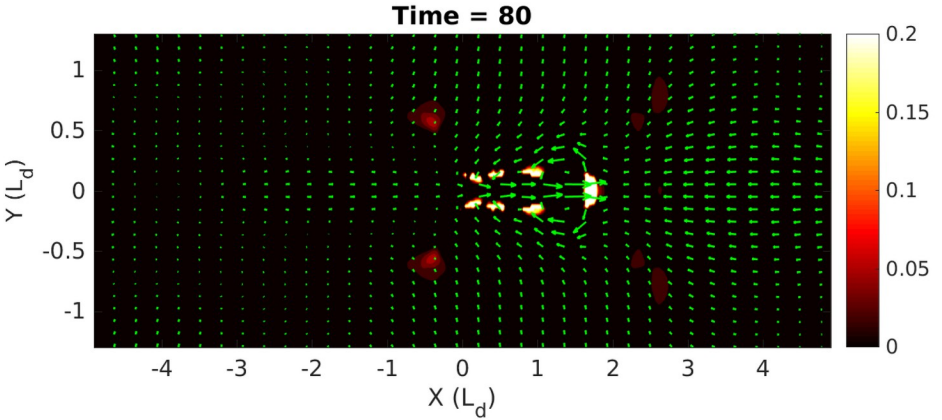

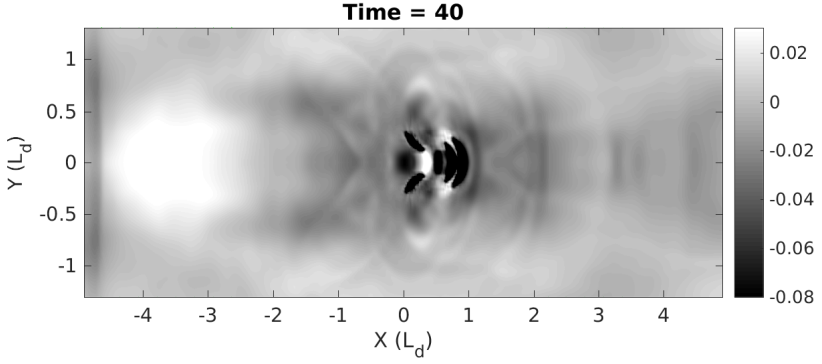

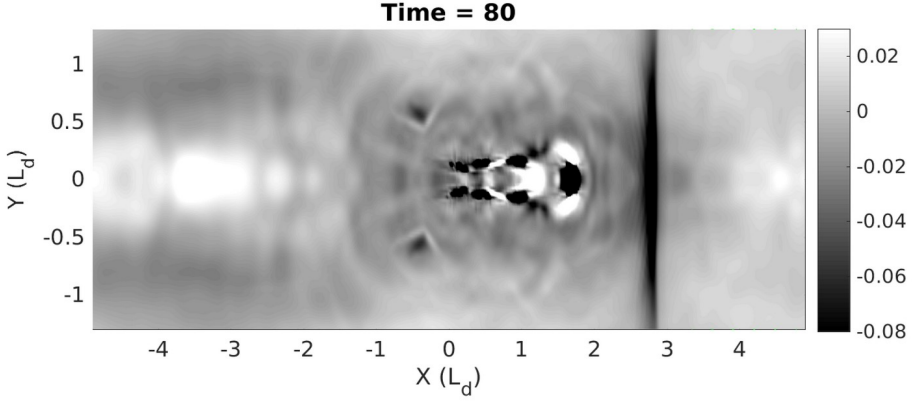

Hovmöller diagram of the ”hybrid structure” due to low pressure anomaly

Left panel: baroclinic zonal velocity

Right panel: zonal velocity in the lower layer

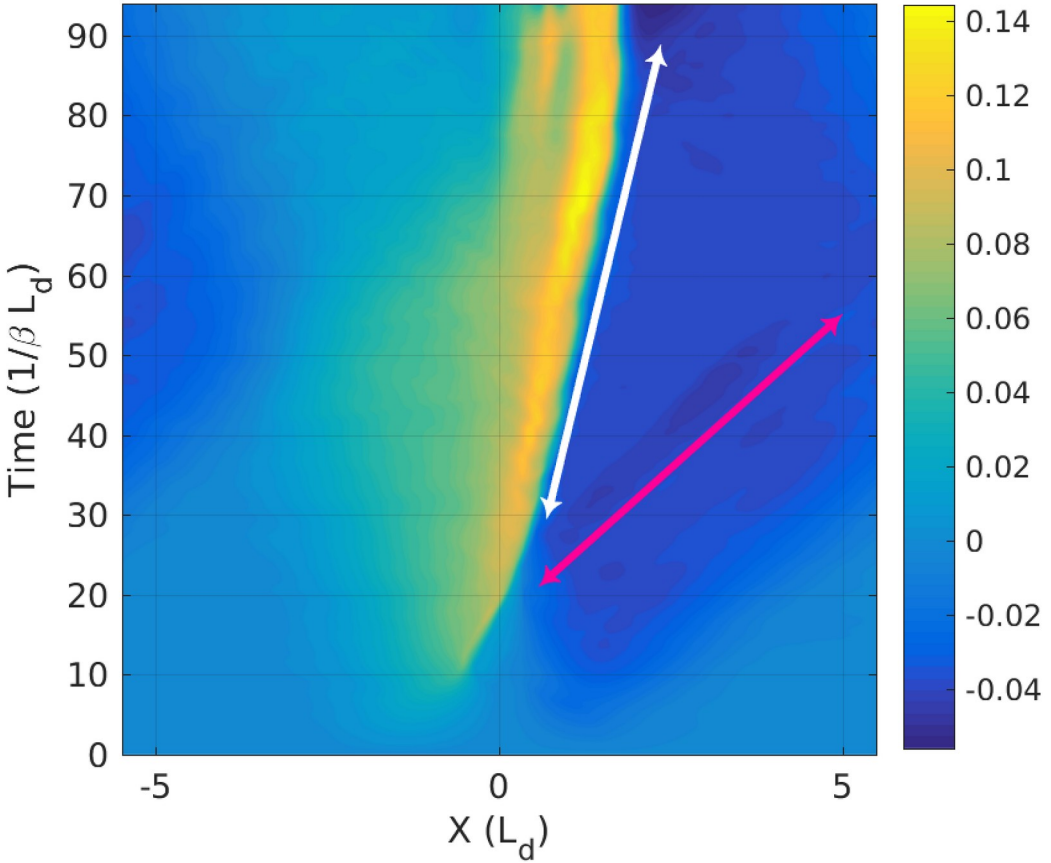

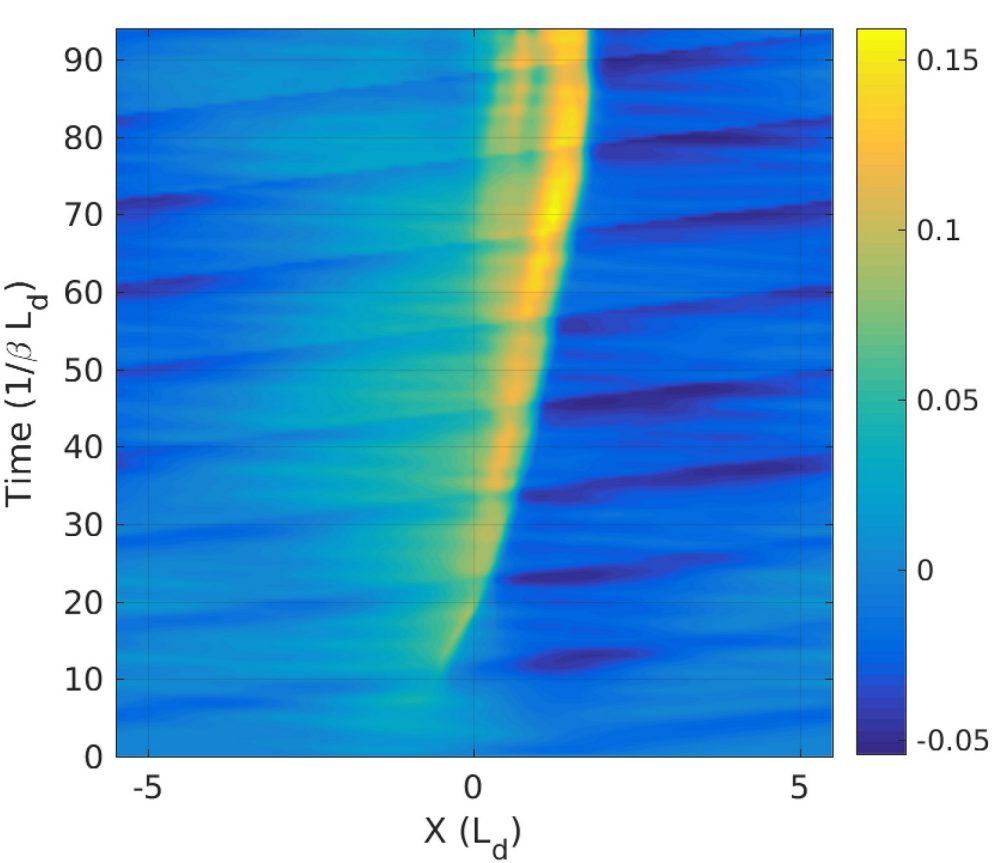

Adjustment of positive buoyancy anomaly via mcTRSW

Evolution of the buoyancy, vorticity, and precipitation in the lower troposphere during eastward propagation:

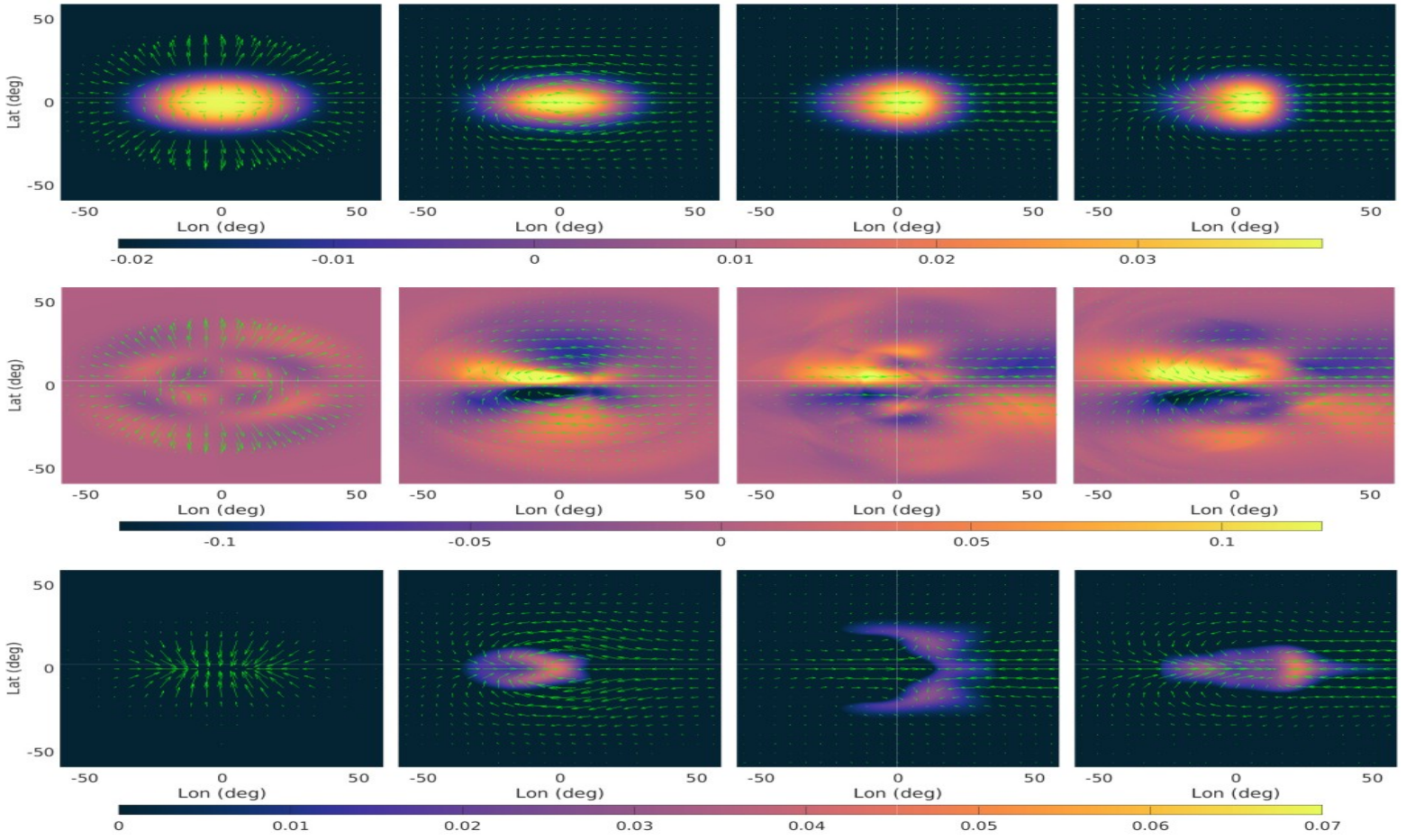

Adjustment of b1 positive anomaly via mcTRSW (Rostami et al., 2022)

Left panel: buoyancy anomaly

Right panel: precipitation

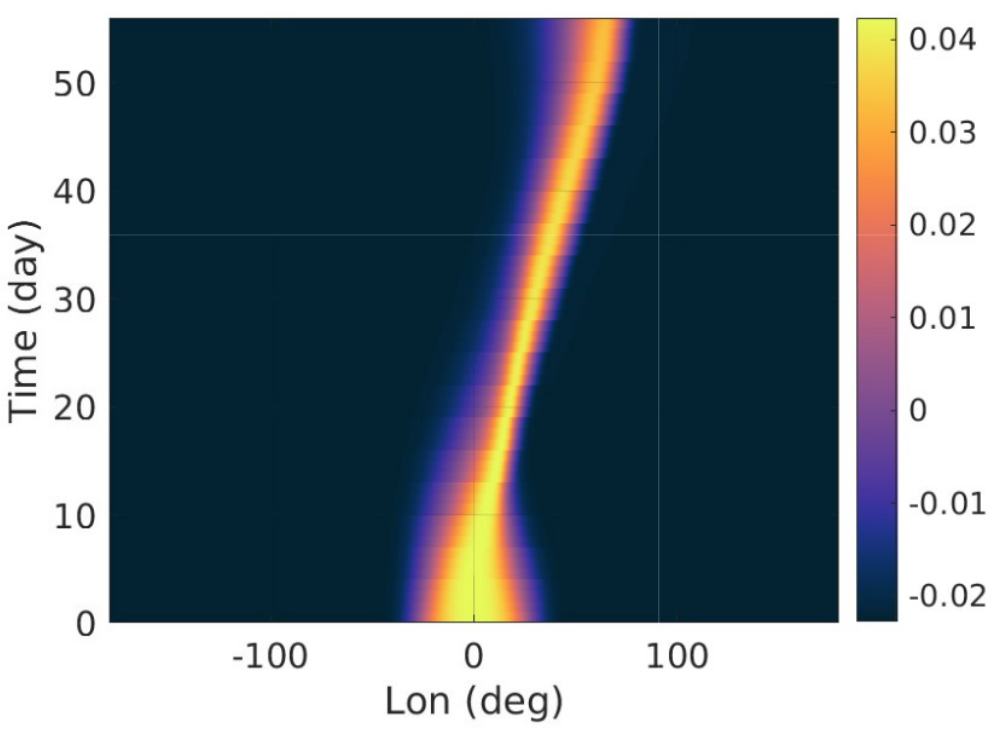

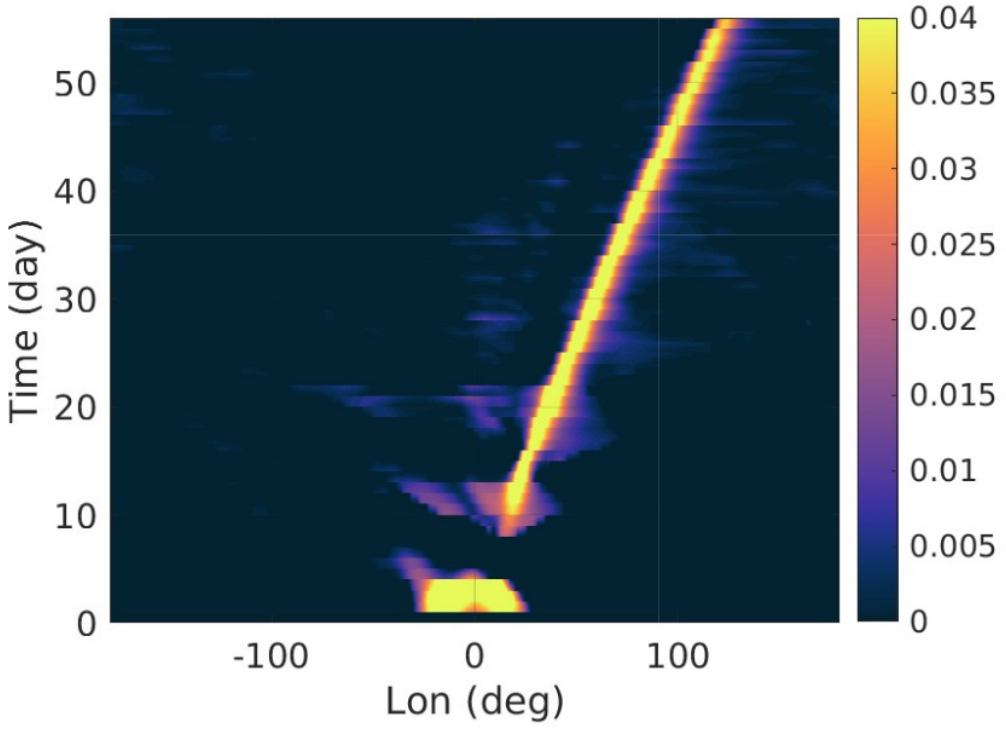

Hovmöller diagram of the ”hybrid structure” due to high buoyancy anomaly (Rostami et al., 2022)

Left panel: zonal velocity in the lower layer

Right panel: baroclinic zonal velocity

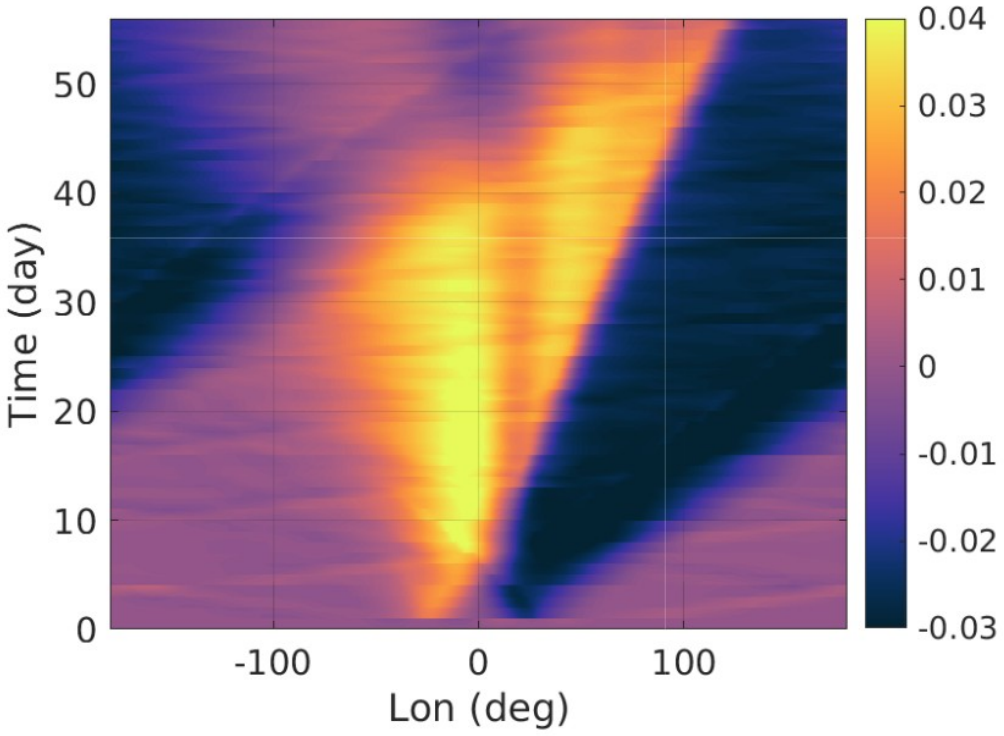

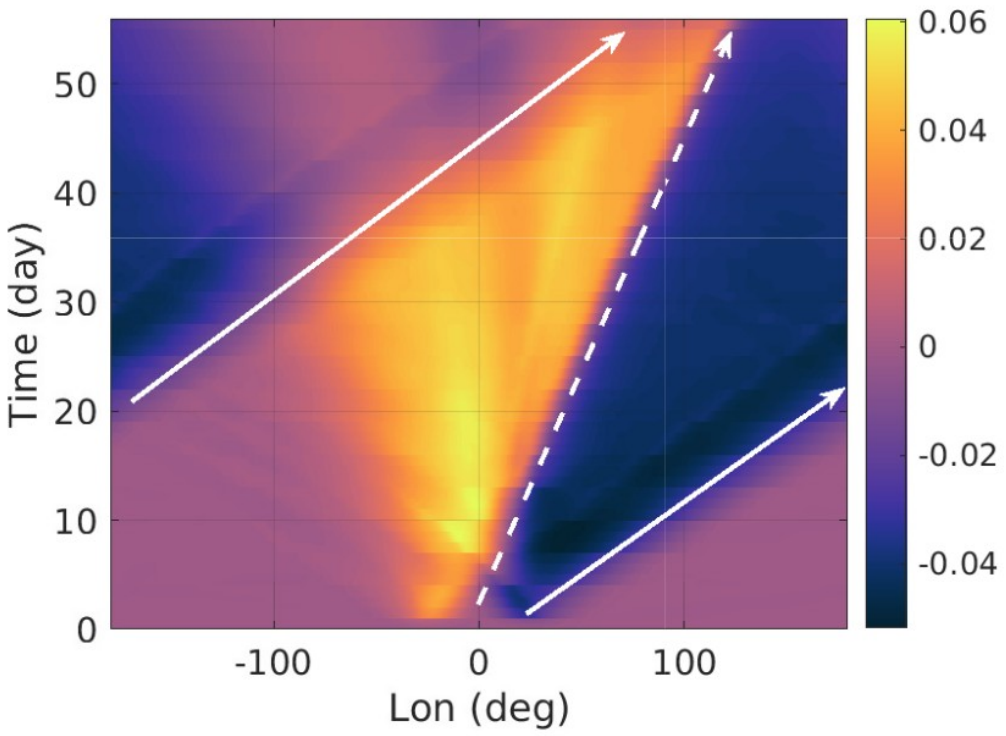

Evolution of pressure anomaly vs. buoyancy anomaly

(Rostami et al., 2022)

Left panel: pressure, vorticity, precipitation

Right panel: buoyancy, vorticity, precipitation

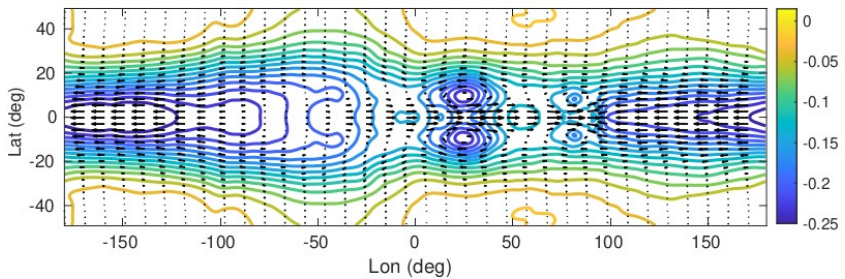

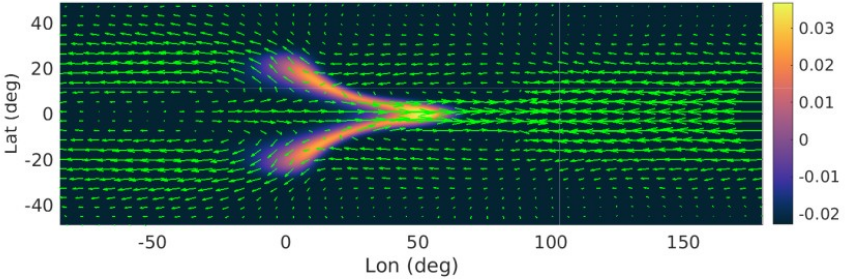

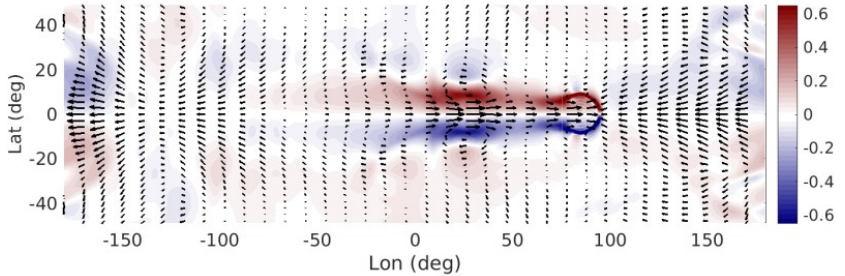

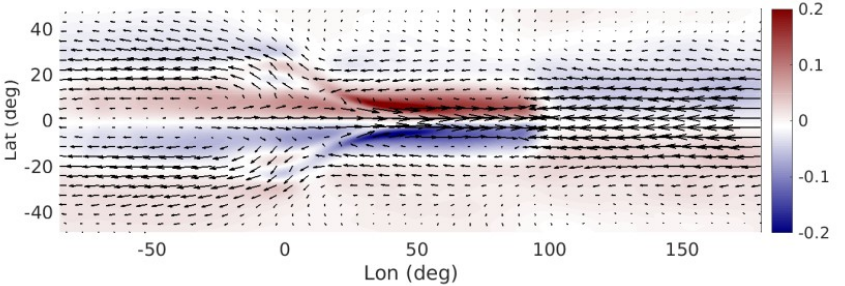

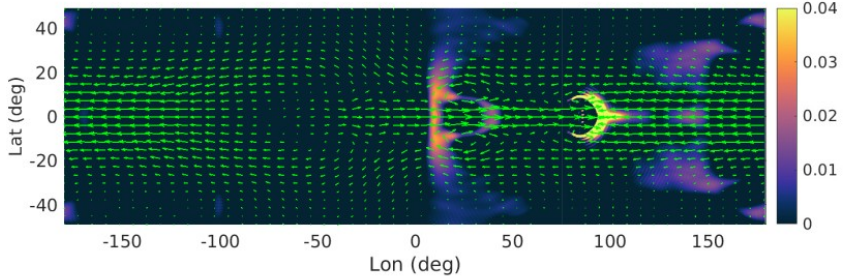

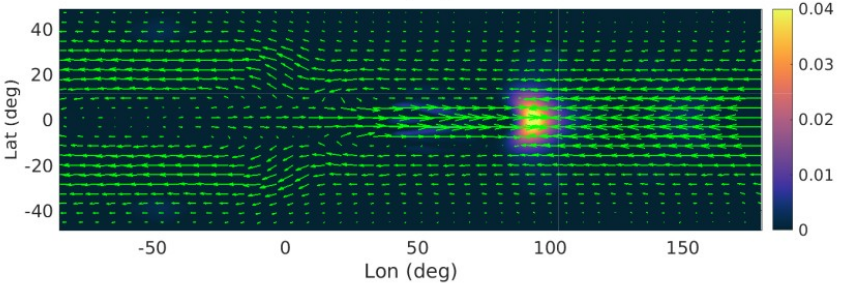

Recurrent generation of MJO-like structure (Rostami et al., 2022)

Passing BKW over a positive buoyancy anomaly with half intensity of previous initial b1 anomaly

Left panel: precipitation

Right panel: baroclinic zonal velocity

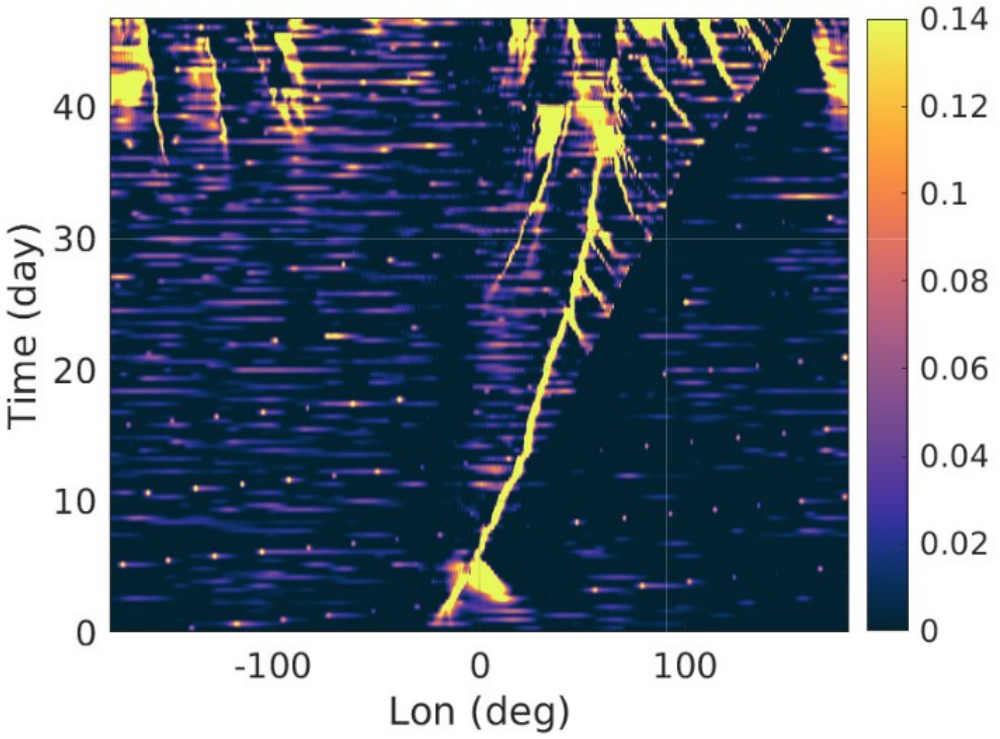

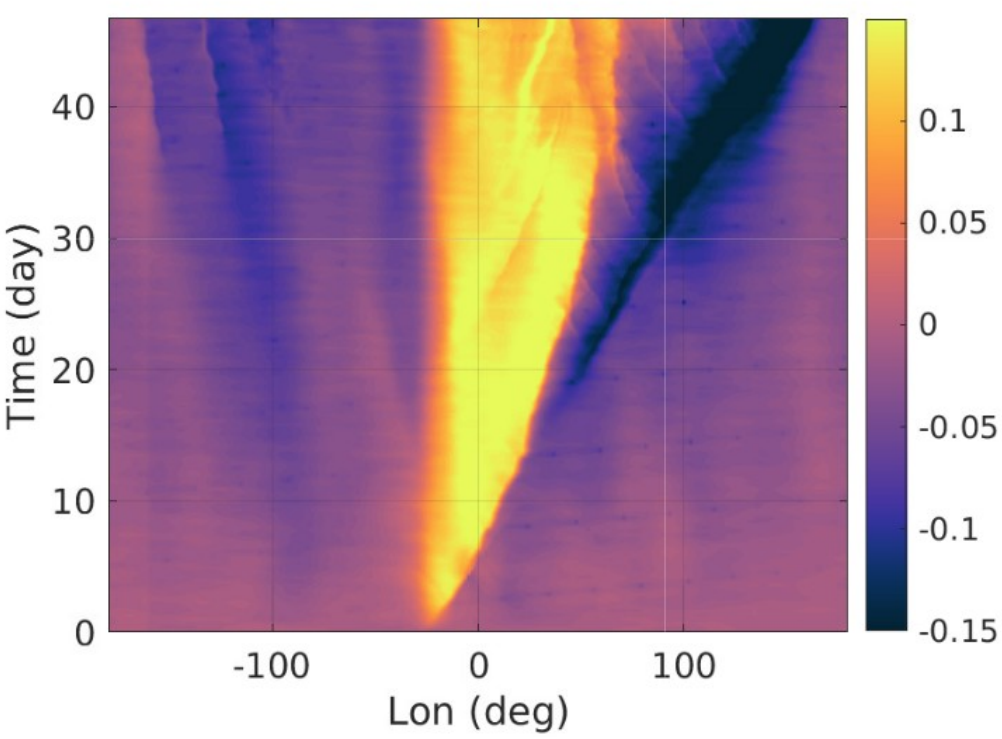

synoptic vs. large-scale meridionally elongated perturbation

(Rostami et al., 2022)

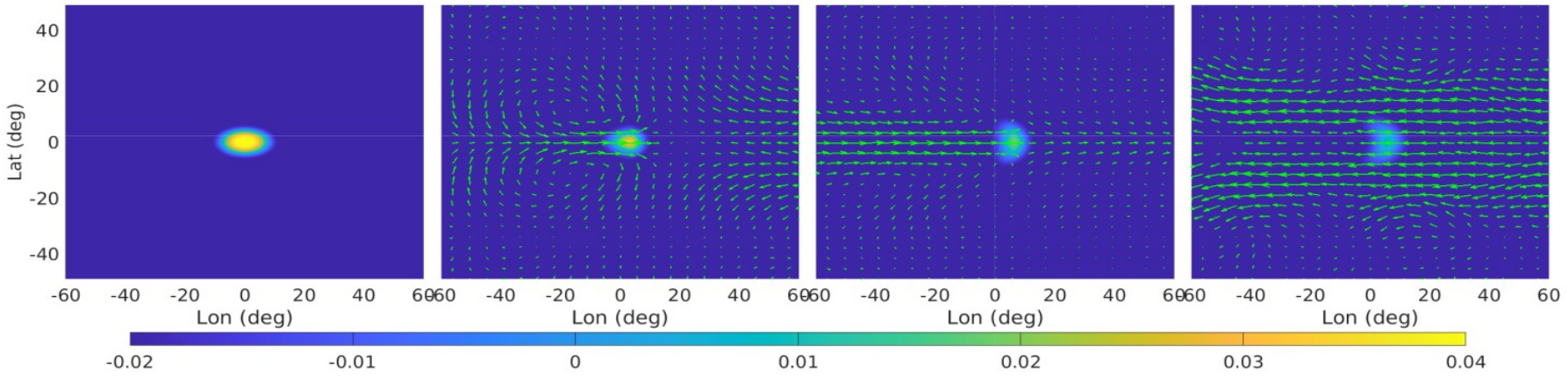

(b)

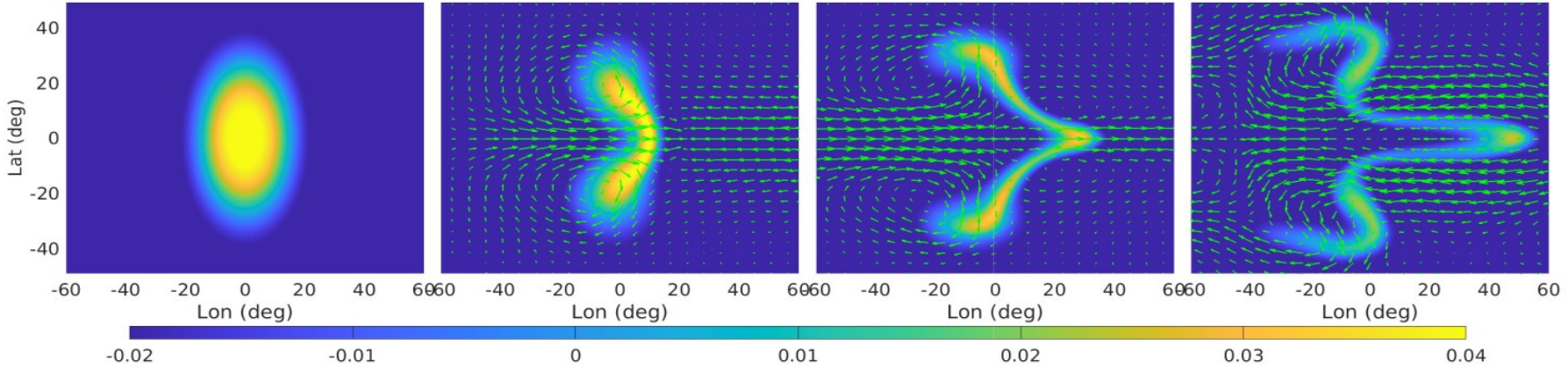

Conclusion

I. According to this theory MJO-like structure can be generated in a self-sustained and self-propelled manner due to ***nonlinear relaxation*** (adjustment) of a large-scale positive buoyancy anomaly, depressed anomaly, or a combination of them, as soon as this anomaly reaches a critical threshold in the presence of moist-convection at the equator.

II. "***hybrid structure***" consists of a "quasi equatorial modon", with an enhanced vortex pair, and a convectively coupled baroclinic Kelvin wave (BKW), with greater phase speed than that of dipolar structure on the intraseasonal time scale.

III. Interaction of the BKW, after circumnavigating all around the equator, with a new large-scale buoyancy anomaly may contribute to excitation of a ***recurrent generation*** of the next cycle of MJO-like structure.

IV. Crudest captured features of the MJO: quadrupolar structure, convective activity, condensation patterns, vorticity field, phase speed, and westerly and easterly inflows in the lower and upper troposphere.

V. We proposed a new multi-layer pseudo-spectral moist-convective Thermal Rotating Shallow Water (***mcTRSW***) model in a full sphere as the dynamical core of Aeolus2.

Moist vs dry characteristic velocities

c^m is real for positive moist enthalpy of the lower layer in the state of rest : $M_1 = H_1 - \beta Q^s > 0$, and

$$C_-^m < C_- < \frac{g(H_1 + \alpha H_2)}{2} < C_+ < C_+^m,$$

for $0 < M_1 < H_1 \Rightarrow$ moist internal (mainly baroclinic) mode propagates slower than the dry one, consistent with observations.

Moist vs dry characteristic velocities

c^m is real for positive moist enthalpy of the lower layer in the state of rest : $M_1 = H_1 - \beta Q^s > 0$, and

$$C_-^m < C_- < \frac{g(H_1 + \alpha H_2)}{2} < C_+ < C_+^m,$$

for $0 < M_1 < H_1 \Rightarrow$ moist internal (mainly baroclinic) mode propagates slower than the dry one, consistent with observations.

Non-universality of Gill's mechanism

Large vs order one aspect ration of disturbance, "Dry" adjustment of circular pressure anomaly.

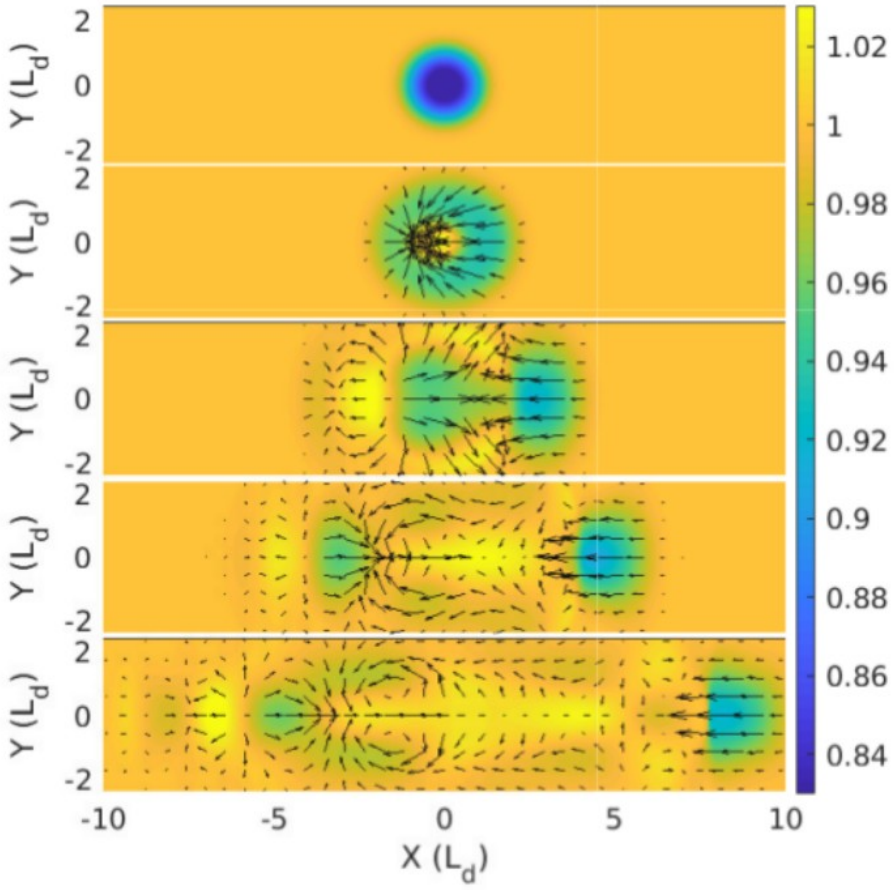

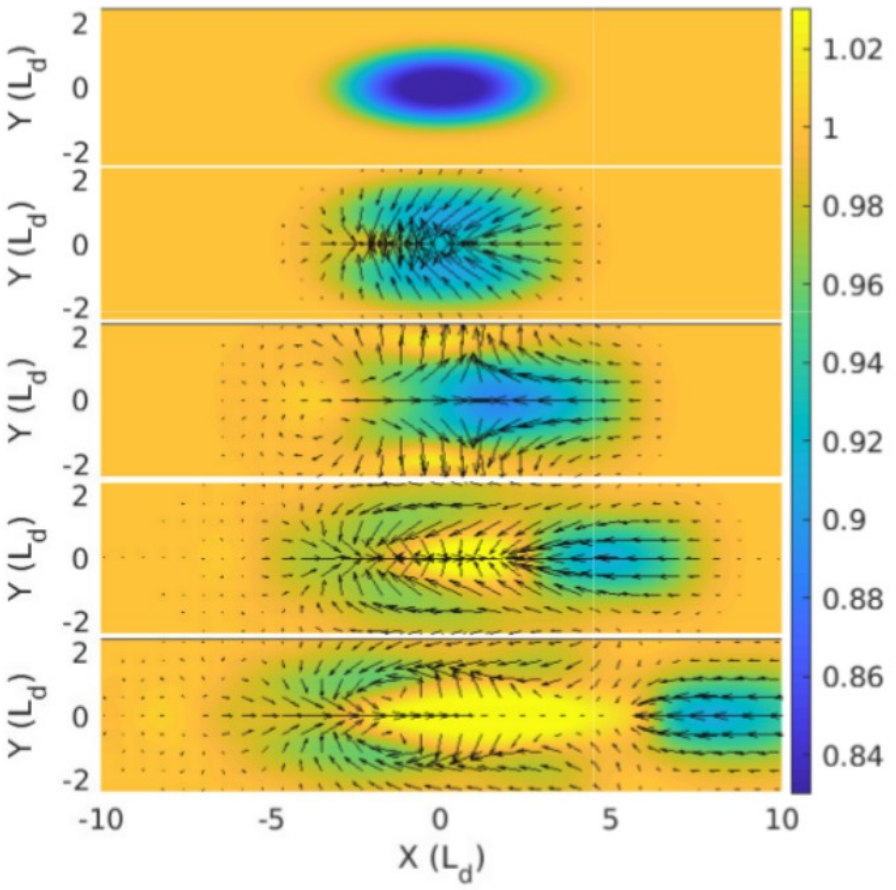

mcRSW vs mcTRSW

Pseudo spectral moist-convective Thermal Rotating Shallow Water model

(Rostami et al.,2021, under preparation).

A summary of derivation of mcTRSW: we start with the atmospheric primitive equations in terms of the pseudo-height isobaric vertical coordinate (Hoskins and Bretherton 1972):

$$\frac{\partial \boldsymbol{v}_h}{\partial t} + (\boldsymbol{v}_h \cdot \boldsymbol{\nabla})\boldsymbol{v}_h + f\hat{\boldsymbol{z}} \times \boldsymbol{v}_h = -\boldsymbol{\nabla}\Phi,$$

$$\frac{\partial \Phi}{\partial z} = g\frac{\theta}{\theta_s},$$

$$\boldsymbol{\nabla}_h \cdot \boldsymbol{v}_h + \frac{\partial w}{\partial z} = 0,$$

$$\frac{\partial \theta}{\partial t} + (\boldsymbol{v}_h \cdot \boldsymbol{\nabla})\theta + w\frac{\partial \theta}{\partial z} = 0,$$

mcRSW vs mcTRSW

Pseudo spectral moist-convective Thermal Rotating Shallow Water model

(Rostami et al.,2021, under preparation).

A summary of derivation of mcTRSW: We will count the layers from bottom to top. We thus get the following master equation:

$$(z_i - z_{i-1})\left(\frac{\partial \boldsymbol{v}_i}{\partial t} + (\boldsymbol{v}_i \cdot \boldsymbol{\nabla})\boldsymbol{v}_i + f\hat{\boldsymbol{z}} \times \boldsymbol{v_i}\right) = -\boldsymbol{\nabla}\left(\frac{1}{2}\frac{g\bar{\theta}_i}{\theta_s}(z_i - z_{i-1})^2 + \Phi(z_{i-1}h_i)\right) + \Phi(z_i)\boldsymbol{\nabla} z_i - \Phi(z_{i-1})\boldsymbol{\nabla} z_{i-1},$$

$$\Phi(z_i) = \Phi(z_{i-1}) + h_i b_i = \Phi(z_0) + \sum_{j=1}^{i} \frac{g\bar{\theta}_j}{\theta_s} h_j = \Phi(z_0) + \sum_{j=1}^{i} h_j b_j$$

mcRSW vs mcTRSW

Pseudo spectral moist-convective Thermal Rotating Shallow Water model

(Rostami et al.,2021, under preparation).

A summary of derivation of mcTRSW:

For each layer of TRSW model the corresponding vertically integrated equations can be written as:

$$\frac{d\boldsymbol{v}_i}{dt} + f\hat{\boldsymbol{z}} \times \boldsymbol{v}_i = b_i \boldsymbol{\nabla} z_i + \frac{1}{2} h_i \boldsymbol{\nabla} b_i - \boldsymbol{\nabla}(\Phi(z_0) + \sum_{j=1}^{i} h_j b_j),$$

$$\frac{\partial h_i}{\partial t} + \boldsymbol{\nabla}(h_i \boldsymbol{v}_i) = 0, \quad 1 < i \leq m; \quad \frac{\partial h_i}{\partial t} + \boldsymbol{\nabla}[(h_i - h_b)\boldsymbol{v}_i] = 0, \quad i = 1,$$

$$\frac{db_i}{dt} = 0,$$

mcRSW vs mcTRSW

Pseudo spectral moist-convective Thermal Rotating Shallow Water model

(Rostami et al.,2021, under preparation).

A summary of derivation of mcTRSW:

For a system of 3-layer TRSW with a rigid lid $\nabla z_m = 0$, momentum equations can be written explicitly as:

$$\frac{d\boldsymbol{v}_1}{dt} + f\hat{\boldsymbol{z}} \times \boldsymbol{v}_1 = \frac{1}{2} h_1 \nabla b_1 - b_1 \nabla (h_2 + h_3) - \nabla \left[\Phi(z_0) + h_1 b_1\right],$$

$$\frac{d\boldsymbol{v}_2}{dt} + f\hat{\boldsymbol{z}} \times \boldsymbol{v}_2 = \frac{1}{2} h_2 \nabla b_2 - b_2 \nabla h_3 - \nabla \left[\Phi(z_0) + h_1 b_1 + h_2 b_2\right],$$

$$\frac{d\boldsymbol{v}_3}{dt} + f\hat{\boldsymbol{z}} \times \boldsymbol{v}_3 = \frac{1}{2} h_3 \nabla b_3 - \nabla \left[\Phi(z_0) + h_1 b_1 + h_2 b_2 + h_3 b_3\right],$$

Thank you for your attention

References

(1) Bouchut, F., Lambaerts, J., Lapeyre, G. & Zeitlin, V. (2009). Fronts and nonlinear waves in a simplified shallow-water model of the atmosphere with moisture and convection. *Physics of Fluids*, 21,116604, https://doi.org/10.1063/1.3265970.

(2) Charney, J., (1963), A note on large-scale motions in the tropics, *Journal of Atmospheric Sciences*, 20, 607.

(3) Holm, D., D., Luesink, E., Pan, W. (2021). Stochastic mesoscale circulation dynamics in the thermal ocean. *Physics of Fluids*, 33, 046603, https://doi.org/10.1063/5.0040026.

(4) Gill, A. (1980), Some simple solutions for heat induced tropical circulation, *Quarterly Journal of the Royal Meteorological Society*, 106, 447–462.

(5) Gelfand, I. M., & Shapiro, Z. Y. (1956). Representations of the group of rotations in three-dimensional space and their applications. *American Mathematical Society*, 2 , 207 – 316, https://books.google.de/books?id=Vtm1YgEACAAJ.

(6) Lecoanet, D., Vasil, G. M., Burns, K. J., Brown, B. P., & Oishi, J. S. (2019). Tensor calculus in spherical coordinates using Jacobi polynomials. Part–II: Implementation and examples. *Journal of Computational Physics: X*, 3 , 100012, https://doi.org/10.1016/j.jcpx.2019.100012.

(7) Matsuno, T. (1966), Quasi-geostrophic motions in the equatorial area, *Journal of the Meteorological Society of Japan*, 44 , 2543.

(8) Rostami, M., and Zeitlin, V., (2016), Influence of condensation and latent heat release upon barotropic and baroclinic instabilities of vortices in rotating shallow water f-plane model. *Geophysical & Astrophysical Fluid Dynamics*, 111 (1), 131, https://doi.org/10.1080/03091929.2016.1269897.

(9) Rostami, M. & Zeitlin, V. (2018). An improved moist-convective rotating shallow-water model and its application to instabilities of hurricane like vortices. *Quarterly Journal of the Royal Meteorological Society*, 144, 1450–1462, https://doi.org/10.1002/qj.3292.

(10) Rostami, M., and Zeitlin, V., (2019), Eastward-moving convection-enhanced modons in shallow water in the equatorial tangent plane. *Physics of Fluids*, 31, 021701, https://doi.org/10.1063/1.5080415.

(11) Rostami, M., and Zeitlin, V., (2020), Eastward-moving Equatorial Modons in Shallow-Water Models of the Tropical Atmosphere. Geophysical & Astrophysical Fluid Dynamics, https://doi.org/10.1080/03091929.2020.1805448.

(12) Rostami, M., and Zeitlin, V., (2019), Geostrophic adjustment on the equatorial beta-plane revisited. *Physics of Fluids*, 31, 081702, https://doi.org/10.1063/1.5110441.

(13) Rostami, M. and Zeitlin, V., (2020), Can geostrophic adjustment of baroclinic disturbances in tropical atmosphere explain MJO events? *Quarterly Journal of the Royal Meteorological Society*, https://doi.org/10.1002/qj.3884.

(14) Rostami, M., Zhao, B. & Petri, S. (2022). On the genesis and dynamics of madden–Julian oscillation-like structure formed by equatorial adjustment of localized heating. *Quarterly Journal of the Royal Meteorological Society*, 148, 3788–3813, https://doi.org/10.1002/qj.4388.

(15) Rostami, M., Severino, L., Petri, S., & Hariri, S. (2023). Dynamics of localized extreme heatwaves in the mid-latitude atmosphere: A conceptual examination. *Atmospheric Science Letters*, e1188, https://doi.org/10.1002/asl.1188.

(16) Vasil, G. M., Lecoanet, D., Burns, K. J., Oishi, J. S., & Brown, B. P. (2019). Tensor calculus in spherical coordinates using Jacobi polynomials. Part–I: Mathematical analysis and derivations. *Journal of Computational Physics: X*, 3 , 100013, https://doi.org/10.1016/j.jcpx.2019.100013.